nature chemical biology

ARTICLES

https://doi.org/10.1038/s41589-019-0304-8

Harnessing the anti-cancer natural product nimbolide for targeted protein degradation

Jessica N. Spradlin[1,2], Xirui Hu[1,2], Carl C. Ward[2,3], Scott M. Brittain[2,4], Michael D. Jones[2,4], Lisha Ou[1,2], Milton To[5], Andrew Proudfoot[6], Elizabeth Ornelas[6], Mikias Woldegiorgis[6], James A. Olzmann[5,7], Dirksen E. Bussiere[2,6], Jason R. Thomas[2,4,8], John A. Tallarico[2,4], Jeffrey M. McKenna[2,4], Markus Schirle[2,4], Thomas J. Maimone[1,2*] and Daniel K. Nomura[1,2,3,5*]

Nimbolide, a terpenoid natural product derived from the Neem tree, impairs cancer pathogenicity; however, the direct targets and mechanisms by which nimbolide exerts its effects are poorly understood. Here, we used activity-based protein profiling (ABPP) chemoproteomic platforms to discover that nimbolide reacts with a novel functional cysteine crucial for substrate recognition in the E3 ubiquitin ligase RNF114. Nimbolide impairs breast cancer cell proliferation in-part by disrupting RNF114-substrate recognition, leading to inhibition of ubiquitination and degradation of tumor suppressors such as p21, resulting in their rapid stabilization. We further demonstrate that nimbolide can be harnessed to recruit RNF114 as an E3 ligase in targeted protein degradation applications and show that synthetically simpler scaffolds are also capable of accessing this unique reactive site. Our study highlights the use of ABPP platforms in uncovering unique druggable modalities accessed by natural products for cancer therapy and targeted protein degradation applications.

Natural products from organisms such as plants and microbes are a rich source of therapeutic lead compounds[1]. The characterization of their biological activities has resulted in myriad medications for a wide range of pathologies including cancer, bacterial and fungal infections, inflammation and diabetes[1]. Among natural products a subset of covalently acting molecules exist that bear electrophilic moieties capable of undergoing essentially irreversible reactions with nucleophilic amino acids in proteins to exert their therapeutic activity. Examples of these natural products include penicillin, which irreversibly inhibits serine transpeptidases inducing anti-bacterial activity, or wortmannin, which covalently modifies a functional lysine on PI3-kinase to inhibit its activity[1,2]. Discovering druggable hotspots targeted by anti-cancer and covalently acting natural products can not only yield new cancer drugs and therapeutic targets but can also reveal unique insights into modalities accessed by natural products in protein targets that are often considered undruggable or difficult to tackle with standard drug discovery efforts. One example of a druggable modality that would be difficult to predict a priori is FK506 or Tacrolimus that inhibits peptidylprolyl isomerase activity by binding to FKBP12 thus creating a FKBP12-FK506 complex that modulates T cell signaling via inhibition of calcineurin[3]. Gaining insights into nature's strategies for engaging protein targets can thus provide access to new perspectives on what may be considered druggable.

In this study, we investigated the mechanism of action of the natural product nimbolide (**1**), a limonoid natural product derived from the Neem tree (*Azadirachta indica*) (Fig. 1a)[4]. Nimbolide has been shown to exert multiple therapeutic effects and possesses a cyclic enone capable of reacting with cysteines[5–7]. In the context of cancer, nimbolide has been shown to inhibit tumorigenesis and metastasis without causing any toxicity or unwanted side effects across a wide range of cancers[8]. While previous studies suggest that nimbolide impairs cancer pathogenicity through modulating signaling pathways and transcription factors linked to survival, growth, invasion, angiogenesis, inflammation and oxidative stress the direct targets of nimbolide still remain poorly characterized[8].

Identifying direct protein targets of complex natural products remains challenging and often requires synthesizing analogs of these compounds bearing photoaffinity and enrichment handles, a task that is synthetically challenging and has the potential to alter the activity of the molecule[1]. Even with the generation of such probes, identifying the specific amino acid site targeted by natural products is challenging. In this study, we used ABPP chemoproteomic approaches to map the proteome-wide targets of nimbolide in breast cancer cell proteomes. Using ABPP platforms, we reveal that one of the primary targets of nimbolide in breast cancer cells is cysteine-8 (C8) of the E3 ubiquitin ligase RNF114. Covalent modification of RNF114 by nimbolide leads to impaired ubiquitination and degradation of its substrate—the tumor suppressor CDKN1A (p21)—leading to its rapid stabilization. We show that this apparent inhibition of RNF114 activity is through impaired substrate recognition, giving rise to the possibility that nimbolide could be used as an E3 ligase recruitment module for targeted protein degradation. Strategies for chemically induced degradation of targets of interest in cells is rapidly gaining interest in drug discovery, including the development of bifunctional molecules referred to as 'proteolysis-targeting chimeras' or 'heterobifunctional degraders' that consist of a protein-targeting ligand linked to an E3 ligase recruiter to bring an E3 ligase to a protein of interest to ubiquitinate and mark the target for degradation in a proteasome-dependent

[1]Department of Chemistry, University of California, Berkeley, Berkeley, CA, USA. [2]Novartis-Berkeley Center for Proteomics and Chemistry Technologies, Berkeley, CA, USA. [3]Department of Molecular and Cell Biology, University of California, Berkeley, Berkeley, CA, USA. [4]Novartis Institutes for BioMedical Research, Cambridge, MA, USA. [5]Department of Nutritional Sciences and Toxicology, University of California, Berkeley, Berkeley, CA, USA. [6]Novartis Institutes for BioMedical Research, Emeryville, CA, USA. [7]Chan Zuckerberg Biohub, San Francisco, CA, USA. [8]Present address: Vertex Pharmaceuticals, Boston, MA, USA. *e-mail: maimone@berkeley.edu; dnomura@berkeley.edu

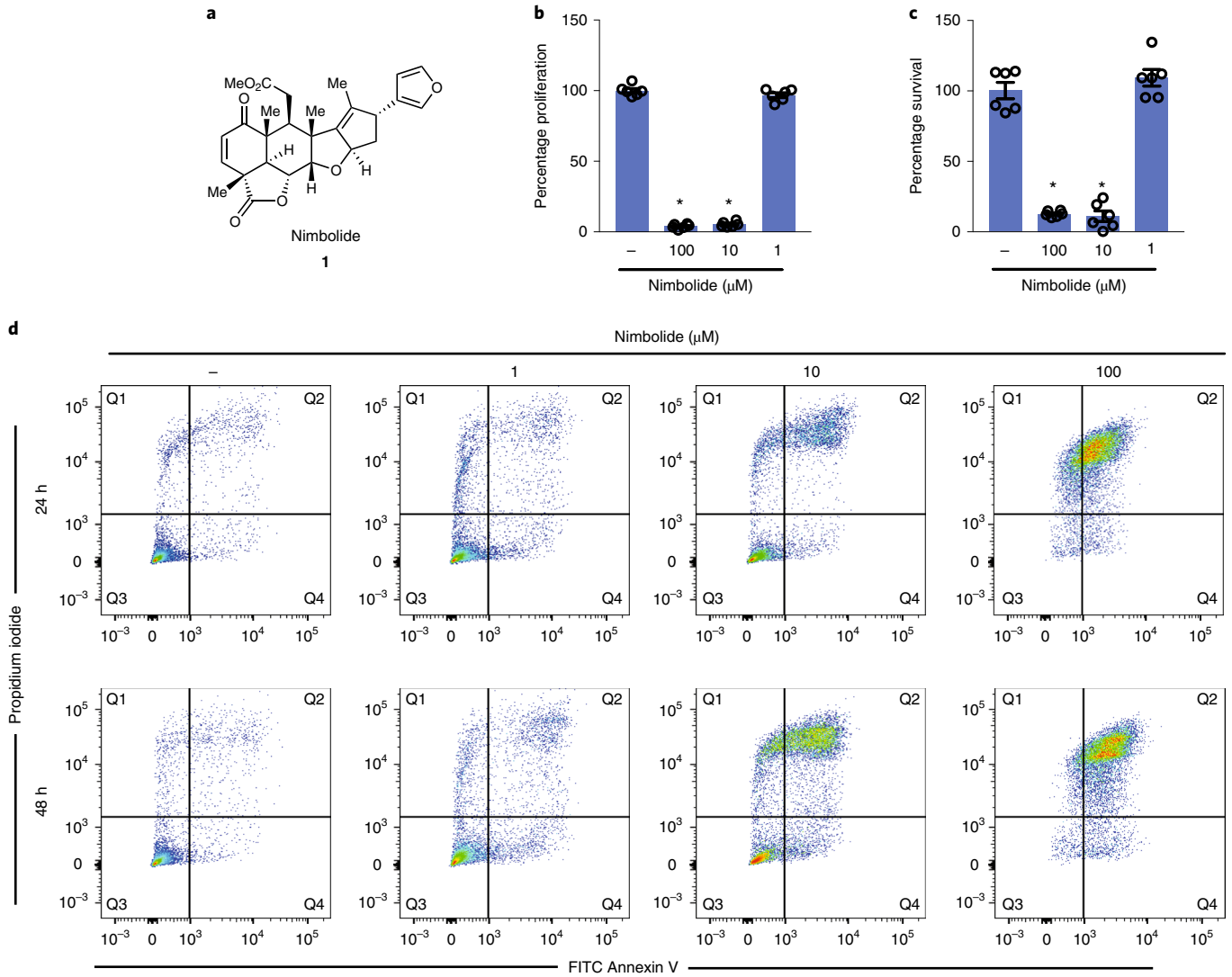

Fig. 1 | Nimbolide impairs breast cancer cell proliferation and survival. a, Structure of nimbolide. Nimbolide possesses a cyclic enone that is potentially cysteine-reactive. **b**,**c**, 231MFP breast cancer cell proliferation in serum-containing media (**b**) and serum-free cell survival (**c**). Data shown in **b** and **c** are mean ± s.e.m.; $n = 6$ biologically independent samples/group. **d**, Percentage of propidium iodide and Annexin V-positive (PI^+/Annexin V^+) cells assessed by flow cytometry after treating 231MFP cells with DMSO vehicle or nimbolide for 24 or 48 h. Shown are representative fluorescence-activated cell sorting data from $n = 3$ biologically independent samples/group. Quantitation of the percentage of late-stage apoptotic cells defined as $FITC^+/PI^+$ cells are shown in Supplementary Fig. 1d. Statistical significance was calculated with unpaired two-tailed Student's *t*-tests. Significance is expressed as $^*P = 7.75 \times 10^{-14}$ and 1.14×10^{-13} for 100 and 10 μM, respectively, in **b** and $^*P = 3.88 \times 10^{-8}$ and 1.53×10^{-7} for 100 and 10 μM, respectively, in **c** compared to vehicle-treated controls.

manner[9,10]. We demonstrate that nimbolide can be used to recruit RNF114 to other protein substrates for targeted protein degradation applications. Using chemoproteomics-enabled covalent ligand screening platforms, we also identify more synthetically tractable compounds that can similarly react with C8 of RNF114 and phenocopy nimbolide action.

Results

Effects of nimbolide on breast cancer phenotypes. Although nimbolide has been shown to impair cancer pathogenicity across many different types of human cancers, we chose to focus on elucidating the role of nimbolide in triple-negative breast cancers (TNBC). TNBCs are devoid of estrogen, progesterone and HER2 receptors, and are among the most aggressive cancers with the worst clinical prognosis[11]. Very few targeted therapies currently exist for TNBC patients. Uncovering new therapeutic modalities in TNBCs would thus potentially contribute to reducing breast cancer-associated mortalities. Consistent with previous reports showing anti-cancer activity in breast cancer cells, nimbolide impaired cell proliferation or serum-free cell survival in 231MFP and HCC38 TNBC cells (Fig. 1b,c and Supplementary Fig. 1a,b)[8]. We also show that these effects on 231MFP and HCC38 viability are due to a significant increase in apoptotic cells with nimbolide treatment, assessed by flow cytometry analysis (Fig. 1d and Supplementary Fig. 1c–e).

ABPP to map nimbolide targets in breast cancer cells. To interrogate the mechanisms by which nimbolide impairs breast cancer pathogenicity, we applied a chemoproteomic platform termed isotopic tandem orthogonal proteolysis-enabled ABPP (isoTOP-ABPP) to determine the specific protein targets of nimbolide. Pioneered by Cravatt and Weerapana, isoTOP-ABPP uses reactivity-based chemical probes to map reactive, functional and

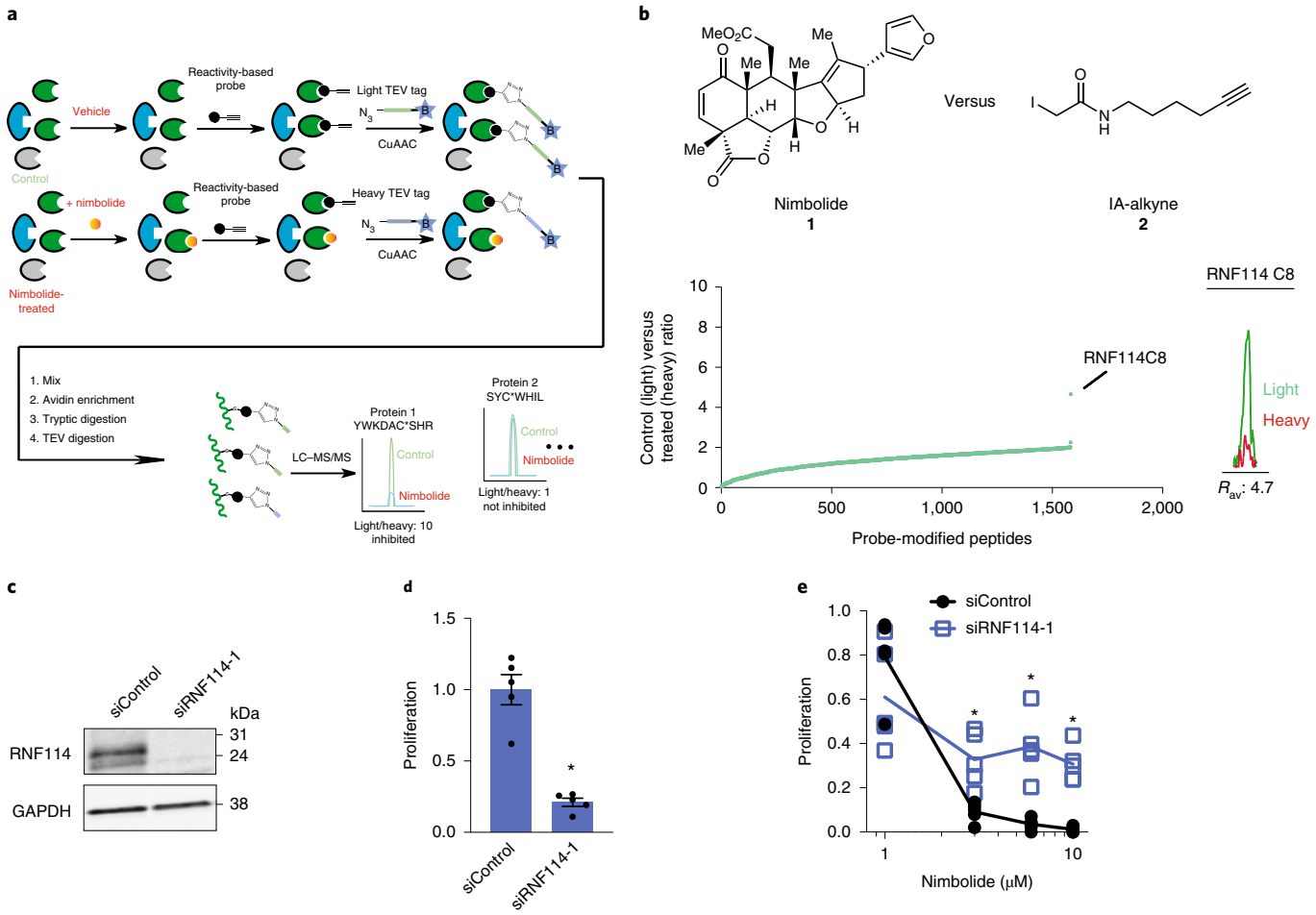

Fig. 2 | isoTOP-ABPP analysis of nimbolide in 231MFP breast cancer cell proteomes reveal RNF114 as a target. a, Schematic of isoTOP-ABPP in which 231MFP breast cancer cells were treated with DMSO or nimbolide (10 μM, 1.5 h in situ), after which cells were collected and proteomes were labeled ex situ with IA-alkyne (100 μM, 1 h) followed by the isoTOP-ABPP procedure. **b**, isoTOP-ABPP analysis of nimbolide (10 μM) in 231MFP breast cancer cells in situ analyzed as described in **a**. Light versus heavy isotopic probe-modified peptide ratios are shown in the left plot in which the primary target with the highest ratio was C8 of RNF114. Shown on the right is a representative MS^1 light versus heavy peak for the probe-modified peptide bearing C8 of RNF114. **c**, RNF114 knockdown by siRNA targeting RNF114 validated by western blotting of RNF114 compared to siControl 231MFP cells. GAPDH expression is shown as a loading control. The shown gel is a representative gel from $n = 3$ biological replicates/group shown in Supplementary Fig. 7a. **d**, 231MFP cell proliferation after 24 h in siControl and siRNF114 cells. **e,** Nimbolide effects on 231MFP siControl and siRNF114 231MFP breast cancer cells. Cells were treated with DMSO vehicle or nimbolide for 24 h after which proliferation was assessed. Data for siControl or siRNF114 group was normalized to the respective DMSO vehicle control in each group. Individual biologically independent sample data is shown and the lines indicate mean values. Data shown in **d** are mean ± s.e.m. Data shown in **b**,**c** are from $n = 3$ and those in **d**,**e** are from $n = 5$ biologically independent samples per group. Statistical significance in **d**,**e** was calculated with unpaired two-tailed Student's *t*-tests. Significance in **d** is expressed as $^*P = 4.52 \times 10^{-5}$ compared to siControl cells. Significance in **e** is expressed as $^*P = 1.90 \times 10^{-5}$, 2.72×10^{-4} and 0.00101 for 10, 6 and 3 μM, respectively, compared to the corresponding nimbolide treatment concentration from siControl groups.

ligandable hotspots directly in complex proteomes[12,13]. When used in a competitive manner, covalently acting small molecules can be competed against binding of broad reactivity-based probes to facilitate the rapid discovery of both proteins and ligandable sites targeted by the covalently acting compound[14–16] (Fig. 2a). In this study, we treated breast cancer cells in situ with vehicle or nimbolide followed by competitive labeling of proteomes with a cysteine-reactive alkyne-functionalized iodoacetamide probe (IA-alkyne) (**2**), after which isotopically light or heavy cleavable enrichment handles were appended to probe-labeled proteins for isoTOP-ABPP analysis. Probe-modified tryptic peptides were analyzed by liquid chromatography–mass spectrometry (LC–MS/MS) and light to heavy tryptic probe-modified peptide ratios, representing control versus treated IA-alkyne labeled sites, were quantified. IsoTOP-ABPP analysis of ligandable hotspots targeted by in situ nimbolide treatment in 231MFP TNBC cells showed one primary target showing an isotopic ratio greater than four that was significantly engaged by nimbolide—the E3 ubiquitin ligase RNF114 (Fig. 2b and Supplementary Dataset 1). RNF114 knockdown using three independent small interfering RNA (siRNA) resembled the anti-proliferative effects of nimbolide in 231MFP cells (Fig. 2c,d and Supplementary Fig. 2a,b). Further demonstrating that RNF114 contributes to the anti-proliferative effects of nimbolide, RNF114 knockdown led to significant resistance to nimbolide-mediated anti-proliferative effects (Fig. 2e and Supplementary Fig. 2c). While nimbolide likely possesses many additional targets beyond RNF114 that are not accessible with isoTOP-ABPP approaches, our results suggested that RNF114 was a novel target of nimbolide and that RNF114 was in part responsible for the anti-proliferative effects of this natural product. We thus chose to

focus further characterization efforts on the interactions between nimbolide and RNF114.

Characterization of nimbolide interactions with RNF114. RNF114 is an E3 ubiquitin ligase of the RING family[17]. The site on RNF114 identified by isoTOP-ABPP as the target of nimbolide, C8, falls inside the N-terminal region of the protein, predicted to be intrinsically disordered and resides outside the two annotated zinc finger domains (Fig. 3a). Intrigued by the apparent targeting of an intrinsically disordered region of a protein by a natural product, we sought to investigate the interaction between nimbolide and RNF114.

Because isoTOP-ABPP is a competitive assay between the covalently acting molecule and a broader reactive probe, it is an indirect read-out of potential nimbolide-targeting hotspots. To confirm that nimbolide directly targeted RNF114, we synthesized the alkyne-functionalized probe shown in three steps from nimbolide (Fig. 3b). Selective bromination at C2 of the furan moiety and subsequent Suzuki coupling with 4-formylphenylboronic acid afforded the aryl-aldehyde (**3**), which was converted to its corresponding carboxylic acid (**4**) via Pinnick oxidation. Finally, coupling of (**4**) and propargylamine (HATU, DIPEA) afforded the target nimbolide-alkyne probe (**5**). We confirmed that this nimbolide probe reacts with pure human RNF114 protein as shown by labeling of the protein on a denaturing SDS–PAGE gel. This labeling event was also competed by nimbolide and abrogated in the C8A RNF114 mutant (Fig. 3c). As the nimbolide-alkyne probe is a synthetically laborious probe that requires the rather expensive nimbolide as a starting material, we also sought to develop a simpler probe that could label C8 of RNF114. In initial studies trying to validate RNF114 interactions with nimbolide, where we competed nimbolide against IA-alkyne labeling of RNF114, full inhibition of labeling was not observed, likely due to alkylation of multiple cysteines by IA-alkyne beyond C8 (Fig. 3d). Thus, we synthesized a more tailored alkyne-functionalized cyclic enone probe JNS27 (**6**), which showed selective labeling of C8 on RNF114 as evidenced by lack of labeling of C8A RNF114 mutant protein (Fig. 3e). With JNS27, we were able to demonstrate full competition of JNS27 labeling with nimbolide with a 50% inhibitory concentration (IC_{50}) of 0.73 μM (Fig. 3e). To demonstrate that nimbolide interactions with RNF114 are not completely driven by reactivity, but rather also through additional interactions with the protein, we show that nimbolide competes against labeling of RNF114 with a rhodamine-functionalized iodoacetamide probe (IA-rhodamine) at far lower concentrations compared to the simpler JNS27 probe or iodoacetamide with an IC_{50} of 0.55, 22 and >100 μM, respectively (Supplementary Fig. 2d). Furthermore, a direct mass adduct of nimbolide was detected on the tryptic peptide containing C8 on RNF114 by LC–MS/MS after incubation of pure protein with the natural product (Supplementary Fig. 2e). All these experiments taken together provide evidence that nimbolide modifies an intrinsically disordered region of RNF114 at C8 through a covalent bond formation.

We next performed two complementary experiments to demonstrate that nimbolide directly engaged RNF114 in 231MFP breast cancer cells. First, we showed dose-responsive nimbolide-alkyne labeling of RNF114 in situ by treating Flag-tagged RNF114 expressing cells with the probe, followed by enrichment of Flag-tagged RNF114 and appending rhodamine-azide onto probe-labeled protein by CuAAC and visualizing by gel-based ABPP methods (Fig. 3f and Supplementary Fig. 2f). We observed robust in situ nimbolide-alkyne labeling with 10 μM of probe, but also observed lower but significant probe labeling even down to 100 nM (Fig. 3f and Supplementary Fig. 2f). Second, we also showed in situ labeling of endogenous RNF114 with the nimbolide-alkyne probe by treating cells with the probe, followed by appending biotin-azide onto probe-labeled proteins by CuAAC and visualizing RNF114 pulldown by western blotting (Fig. 3g). In this case, significant pulldown was observed at 50 μM of the nimbolide-alkyne probe but not lower concentrations. In this experiment, we show that an unrelated protein such as glyceraldehyde 3-phosphate dehydrogenase (GAPDH) is not enriched by the nimbolide-alkyne probe (Fig. 3g). Using these latter conditions, we also performed a complementary quantitative proteomic profiling study to identify any additional proteins that may be enriched from in situ labeling of 231MFP cells with the nimbolide-alkyne probe (Supplementary Dataset 2). Due to acute cytotoxicity issues, we were not able perform in situ competition studies with higher concentrations of nimbolide itself. In this study, we showed that RNF114 was one of the proteins enriched by the nimbolide-alkyne probe more than ten-fold compared to no-probe controls. We also identified 114 additional proteins that were enriched by the probe more than ten-fold compared to no-probe controls. These proteins represent additional potential covalent or non-covalent targets that may contribute to the anti-proliferative effects of nimbolide. These enriched targets may also represent proteins with low to partial degrees of engagement with nimbolide, whereas isoTOP-ABPP experiments are meant to identify higher engagement targets. Additionally, these proteins may include probe-specific targets or proteins that may be enriched indirectly through interactions with direct nimbolide-labeled proteins (Supplementary Dataset 2). Nonetheless, we show that RNF114 is engaged by the nimbolide-alkyne probe in breast cancer cells, even down to 100 nM, and that the anti-proliferative effects of nimbolide are at least in-part mediated by RNF114.

Effects of nimbolide on RNF114 function. RNF114 has been previously shown to ubiquitinate and degrade the tumor suppressor p21, among other substrates[17–19]. In an in vitro reconstituted system, nimbolide inhibited both RNF114 auto-ubiquitination and p21 ubiquitination activity (Fig. 4a,b and Supplementary Fig. 3a,b). The RNF114 C8A mutation did not affect basal RNF114 auto-ubiquitination activity, but attenuated the inhibition observed with nimbolide treatment (Fig. 4c and Supplementary Fig. 3c). Previous characterization of RNF114 suggested that the N terminus may be involved in substrate recognition[17]. Consistent with this premise, we found that the amount of p21 co-immunoprecipitated with RNF114 was reduced by nimbolide, suggesting that the apparent inhibition of RNF114 may be due to impaired substrate recognition, rather than inhibition of its catalytic activity (Fig. 4d and Supplementary Fig. 3d). We further demonstrated that nimbolide treatment in 231MFP cells stabilized CDKN1A (p21) protein expression within 1 h in a dose-responsive manner, with no significant changes to TP53 (p53) levels (Fig. 4e and Supplementary Fig. 3e,f). The elevated levels of CDKN1A observed were not due to transcriptional down-regulation of messenger RNA levels, as p21 mRNA levels remained unchanged with nimbolide treatment (Supplementary Fig. 3g). To identify other potential substrates of RNF114, we also performed a tandem mass tagging (TMT)-based quantitative proteomic experiment on 231MFP cells treated with nimbolide. Consistent with our western blotting data, we observed CDKN1A (p21) as one of the proteins that were significantly elevated more than two-fold with nimbolide treatment (Fig. 4f and Supplementary Dataset 3). We also observed the levels of several other targets that were heightened by nimbolide treatment, including CDKN1C (p57), PEG10 and CTGF. Beyond CDKN1A (p21) and CDKN1C (p57) that have previously been reported as potential RNF114 substrates[17], we conjectured that PEG10 and CTGF may also represent additional novel substrates of RNF114 (Fig. 4f and Supplementary Dataset 3). Consistent with this premise, we demonstrated in an in vitro RNF114 ubiquitination assay that RNF114 ubiquitinates PEG10 and CTGF and that this ubiquitination is inhibited by nimbolide (Fig. 4g). As both p21 and p57 are tumor suppressors that, when elevated, promote cell cycle arrest and apoptosis[20,21], we postulated that the stabilization of both

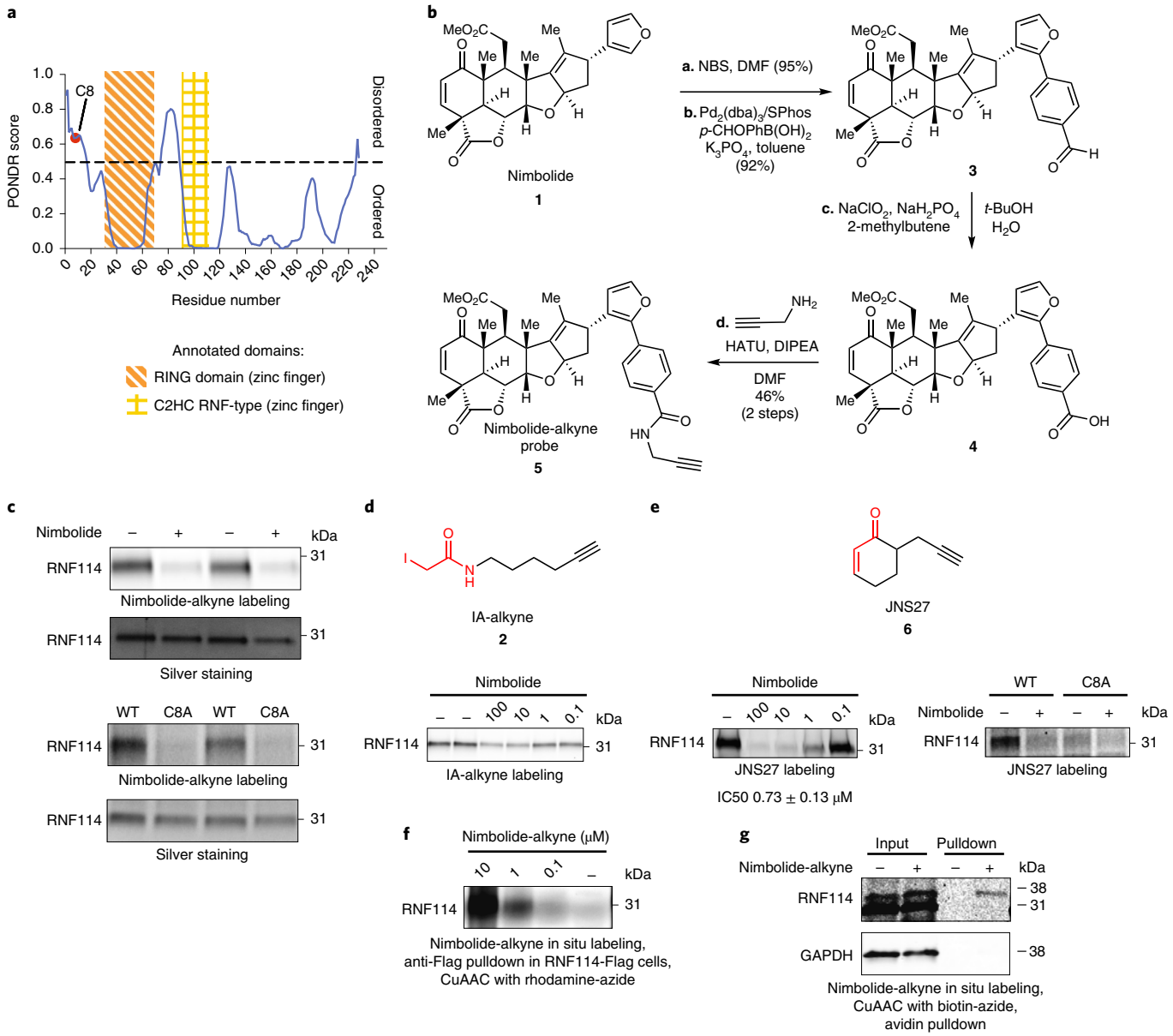

Fig. 3 | Nimbolide reacts covalently with C8 of RNF114. a, Nimbolide targets an intrinsically disordered region in RNF114 as assessed by PONDR. **b**, Route for synthesis of the alkyne-functionalized nimbolide probe. **c**, Gel-based ABPP analysis of pure human RNF114 protein labeled with nimbolide probe. In the upper two panels, pure RNF114 protein was pre-incubated with DMSO vehicle or nimbolide (100 μM, 30 min) before labeling with the nimbolide probe (10 μM, 1 h) in PBS. In the lower two panels, pure wild-type (WT) and C8A mutant RNF114 protein were labeled with the nimbolide probe (10 μM, 1 h) in PBS with 1 mg ml^{-1} BSA. Full-length and replicate blots can be found in Supplementary Fig. 7d,e. **d**, Gel-based ABPP analysis of nimbolide competition against IA-alkyne (10 μM) or JNS27 (50 μM) labeling of pure RNF114 protein. Structures of IA-alkyne and JNS27 probes are shown with reactive moieties highlighted in red. Also shown is gel-based ABPP analysis of nimbolide (50 μM) competition against JNS27 labeling of wild-type and C8A mutant RNF114 protein. In these experiments, DMSO or nimbolide was pre-incubated for 30 min before probe labeling for 1 h. Full-length and replicate blots can be found in Supplementary Fig. 7g,h. **e**, Nimbolide-alkyne labeling of Flag-RNF114 in 231MFP cells. 231MFP cells stably expressing a Flag-tagged RNF114 were treated with DMSO vehicle or nimbolide-alkyne for 2 h. RNF114 was subsequently enriched from collected cell lysates and then rhodamine-azide was appended onto probe-labeled proteins by CuAAC, after which nimbolide-alkyne labeling was visualized by SDS–PAGE and in-gel fluorescence. Full-length and replicate blots can be found in Supplementary Fig. 7i. **f**, Nimbolide-alkyne labeling of endogenous RNF114 in 231MFP cells. 231MFP cells were treated with DMSO vehicle or nimbolide-alkyne (50 μM) for 1.5 h. Biotin-azide was appended to probe-labeled proteins by CuAAC and these proteins were subsequently avidin-enriched. Resulting pulled down proteins were analyzed by SDS–PAGE and western blotting for RNF114. Full-length and replicate blots can be found in Supplementary Fig. 7j Gels shown in **c**–**f** are representative gels from $n = 3$ biologically independent samples/group.

of these tumor suppressors may be responsible for the anti-proliferative effect of nimbolide. We demonstrated that dual knockdown of CDKN1A (p21) and CDKN1C (p57) results in significant attenuation in nimbolide-mediated anti-proliferative effects in 231MFP breast cancer cells (Fig. 4h,i). Collectively, these data suggest that nimbolide reacts with an intrinsically disordered C8 of RNF114 in breast cancer cells to disrupt RNF114-substrate recognition, leading to inhibition of ubiquitination of its substrates such as CDKN1A and CDKN1C, leading to their stabilization and impaired cell proliferation in breast cancer cells.

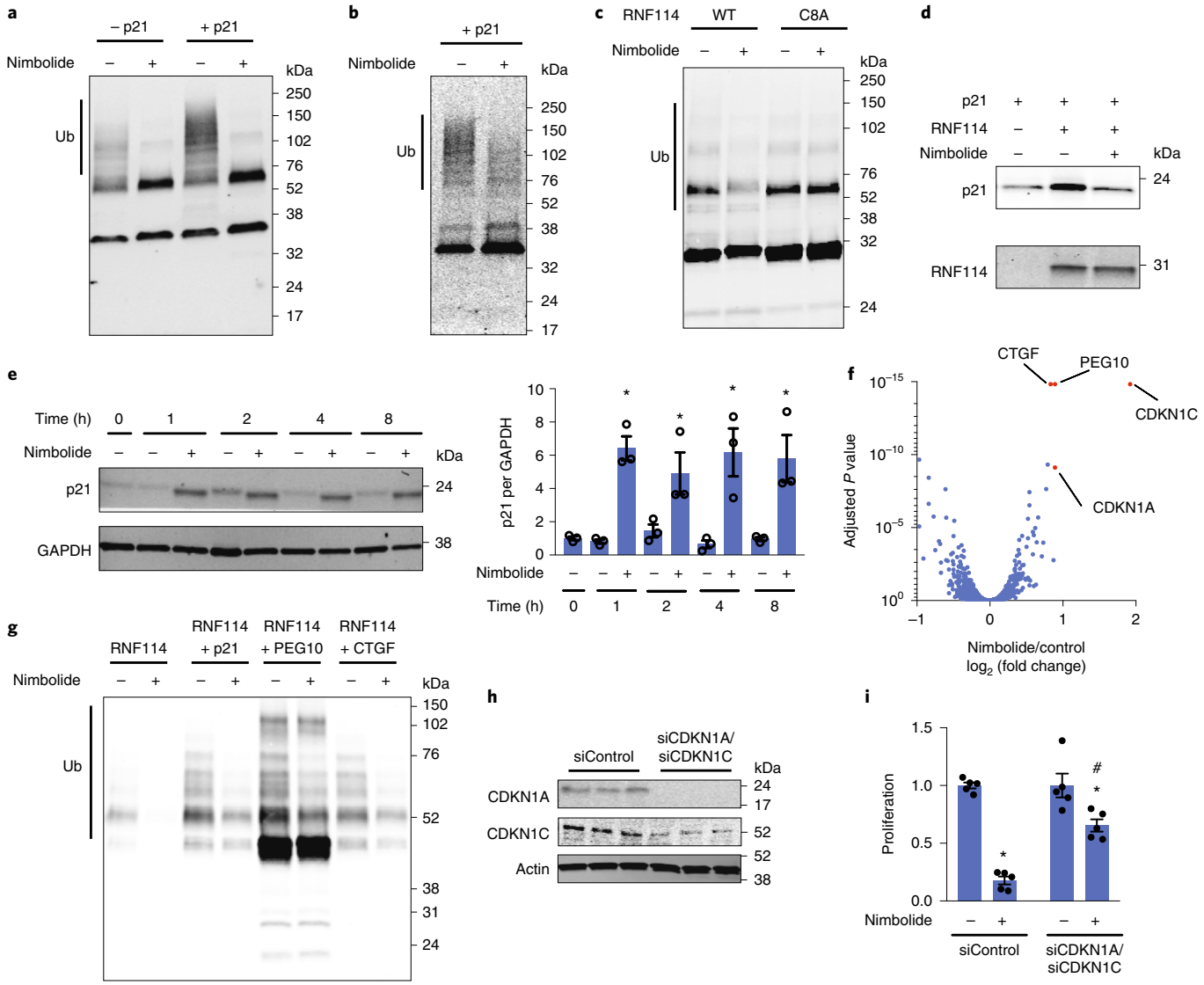

Fig. 4 | Nimbolide inhibits RNF114 activity through disrupting substrate recognition. a,**b**, RNF114 ubiquitination assay with pure GST-Ube1, GST-UBE2D1 and RNF114 protein, Flag-ubiquitin and ATP with or without addition of p21 and blotting against Flag-ubiquitin (**a**) or p21 (**b**). **c**, RNF114 auto-ubiquitination assay with DMSO or nimbolide (100 μM) treatment with wild-type (WT) or C8A mutant RNF114. **d**, In an in vitro incubation of pure RNF114 and p21 protein, Flag-RNF114 pulldown and p21 enrichment were inhibited by nimbolide (100 μM). Full-length and replicate blots can be found in Supplementary Fig. 8a. **e**, 231MFP cells were treated with nimbolide (100 μM). Shown are p21 levels in DMSO control or nimbolide-treated cells. Full-length and replicate blots can be found in Supplementary Fig. 8b. **f**, TMT-based quantitative proteomic profiling of 231MFP breast cancer cells treated with DMSO vehicle or nimbolide (100 nM) for 12 h. Shown in red are proteins that are significantly heightened in levels >two-fold. Data shown in **f** are for 6,397 proteins quantified with two or more unique peptides in $n=3$ biologically independent samples per group, see Supplementary Dataset 3 for details. **g**, RNF114 ubiquitination assay with pure GST-Ube1, GST-UBE2D1 and RNF114 protein, Flag-ubiquitin and ATP with the addition of p21 (CDKN1A), PEG10 or CTGF and blotting against Flag-ubiquitin. DMSO or nimbolide (100 μM) was pre-incubated with RNF114, before the addition of the E1 and E2 enzymes, Flag-ubiquitin and ATP to start the reaction. **h**, p21 (CDKN1A) and p57 (CDKN1C) expression in siControl and siCDKN1A/siCDKN1C 231MFP cells, assessed by western blotting, alongside actin as a loading control. Full-length and replicate blots can be found in Supplementary Fig. 8c. **i**, 231MFP cell proliferation in siControl or siCDKN1A/siCDKN1C cells treated with DMSO vehicle or nimbolide (6 μM) for 24 h. Gels shown in **a**–**e**,**g** are representative images from $n=3$ biologically independent samples/group. Quantification for blots shown in **a**–**d** are in Supplementary Fig. 3a–d. All three biologically independent samples/group are shown in **h**. Data shown in **i** are mean ± s.e.m., $n=5$ biologically independent samples/group. Statistical significance was calculated with unpaired two-tailed Student's *t*-tests in **e** and **i**. Significance is expressed as $^*P=000799$, 0.0295, 0.00962 and 0.0135 for 1, 2, 4 and 8 h, respectively, compared to vehicle-treated control groups for each time point in **e**, and $P=5.65\times10^{-8}$ and 0.0173 compared to vehicle-treated siControl and siCDKN1A/siCDKN1C groups, respectively, in **i**. Significance expressed as $\#P=6.70\times10^{-5}$ compared to nimbolide-treated siControl cells in **i**.

Nimbolide as an RNF114 recruiter. Since nimbolide targets a potential substrate recognition site, we conjectured that nimbolide could be used to recruit RNF114 to other protein substrates for proteasomal degradation through the development of hetero-bifunctional degraders using nimbolide as an RNF114 recruiter. To demonstrate feasibility, two degraders formed by linking nimbolide to the Bromodomain and extra-terminal (BET) family inhibitor JQ1 were synthesized (Fig. 5a and Supplementary Fig. 4a). Previous studies have demonstrated efficient proteasome-dependent degradation of BET family members and in particular BRD4 with JQ1-based degraders linked to either a CRBN (cereblon)-recruiter thalidomide or a von Hippel-Lindau disease tumor suppressor

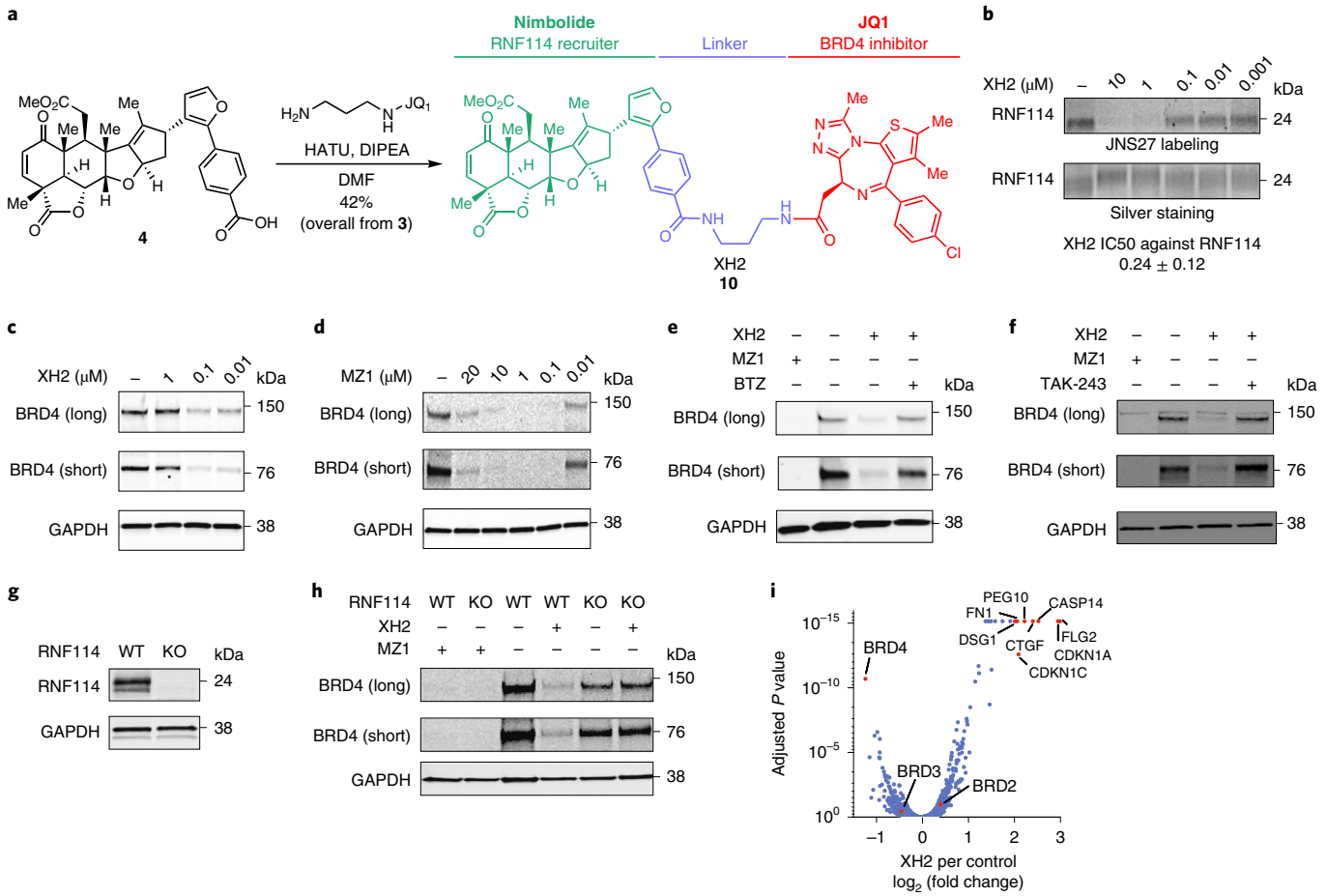

Fig. 5 | Nimbolide can be used to recruit RNF114 for targeted protein degradation of BRD4. a, Route for synthesizing XH2, a nimbolide-based degrader consisting of nimbolide as an RNF114 recruiter, a linker and the BRD4 inhibitor JQ1. **b**, Gel-based ABPP analysis of XH2 against RNF114. RNF114 was pre-incubated with DMSO vehicle or XH2 for 30 min before JNS27 labeling (50 μM) for 1 h followed by appending rhodamine-azide by CuAAC, SDS–PAGE and analysis of in-gel fluorescence. Full-length and replicate blots can be found in Supplementary Fig. 9a. **c**,**d**, BRD4 expression in 231MFP breast cancer cells treated with XH2 (**c**) versus MZ1 (**d**) treatment for 12 h. Full-length and replicate blots can be found in Supplementary Fig. 9b,c. **e**,**f**, BRD4 expression in 231MFP breast cancer cells. Cells were pre-treated with DMSO vehicle or proteasome inhibitor bortezomib (BTZ) (1 μM) (**e**) or E1 ubiquitin-activating enzyme inhibitor TAK-243 (10 μM) (**f**) 30 min before and also during treatment with MZ1 (1 μM) or XH2 (100 nM) for 12 h. Full-length and replicate blots can be found in Supplementary Fig. 9d,e. **g**, RNF114 and loading control GAPDH expression in RNF114 wild-type (WT) and knockout (KO) HAP1 cells. Full-length and replicate blots can be found in Supplementary Fig. 10a. **h**, RNF114 and BRD4 expression in RNF114 wild-type or knockout HAP1 cells treated with DMSO vehicle, MZ1 (1 μM) or XH2 (100 nM) for 12 h. Full-length and replicate blots can be found in Supplementary Fig. 10b. **i**, TMT-based quantitative proteomic profiling of 231MFP breast cancer cells treated with DMSO vehicle or XH2 (100 nM) for 12 h. Long and short BRD4 isoforms in **c**–**h** were visualized by SDS–PAGE and western blotting, quantified by densitometry and normalized to GAPDH loading controls. Gels shown in **b**–**h** are representative images from $n = 3$ biologically independent samples/group and quantification for blots in **c**–**f**,**h** are shown in Supplementary Fig. 4c–f,i. Data shown in **i** are for 5,797 proteins quantified with two or more unique peptides in triplicate treatments, see Supplementary Dataset 3 for details. Statistical significance in **i** are described in the Methods section, and *P* values are reported in Supplementary Dataset 3.

(VHL) recruiter[22,23]. Previously prepared acid (**4**) was coupled to JQ1-functionalized amines containing both longer (PEG-based) (**7**) and shorter (alkyl-based) (**8**) spacer units, arriving at degraders XH1 (**9**) and XH2 (**10**) (Fig. 5a and Supplementary Fig. 4a). We show that XH2 still binds to RNF114 with an IC_{50} of 0.24 μM (Fig. 5b). While XH1 did not show appreciable BRD4 degradation, XH2 treatment in 231MFP cells led to BRD4 degradation after a 12 h treatment (Fig. 5c and Supplementary Fig. 4b). XH2 showed less degradation at 1 μM compared to 0.1 and 0.01 μM and MZ1 showed less degradation at 20 μM compared to 10, 1 and 0.1 μM, which we attribute to the 'hook effect' previously reported with other degraders including the previously reported JQ1-based degrader MZ1 that uses a VHL recruiter[9,22] (Fig. 5c,d). To confirm proteasome-dependence of BRD4 degradation, we showed that the XH2-mediated degradation of BRD4 was attenuated by pre-treatment of cells with the proteasome inhibitor bortezomib (BTZ) (Fig. 5e). XH2-mediated BRD4 degradation was also prevented by pre-treatment with an E1 ubiquitin-activating enzyme inhibitor (TAK-243) or pre-competing with the BRD4 inhibitor JQ1 (Fig. 5f and Supplementary Fig. 4g). However, treatment with a translation inhibitor (emetine) had no effect of the observed degradation of BRD4 (Supplementary Fig. 4h). To further demonstrate that the degradation of BRD4 by XH2 was through the specific recruitment of RNF114, we showed that degradation of BRD4 by XH2, but not MZ1, was not observed in RNF114 knockout HAP1 cells compared to wild-type HAP1 cell counterparts (Fig. 5g,h and Supplementary Fig. 4i). We further showed that re-expression of wild-type RNF114 in HAP1 RNF114 knockout cells led to the restoration of BRD4 degradation by XH2 (Supplementary Fig. 4j). The selectivity of XH2-mediated degradation of proteins was demonstrated using TMT-based quantitative

proteomic profiling experiment to assess changes in protein expression. We showed that XH2 selectively degrades BRD4 in 231MFP breast cancer cells while sparing the other identified BET family members BRD2 and BRD3 (Fig. 5i and Supplementary Dataset 3). Of note, we also observed several proteins that showed increased levels on XH2 treatment including CDKN1A, CDKN1C, PEG10 and CTGF, which were observed as elevated in levels with nimbolide treatment alone (Fig. 5i and Supplementary Dataset 3). There were also additional proteins that were upregulated, such as DSG1, FN1, FLG2 and CASP14 (Fig. 5i and Supplementary Dataset 3). These upregulated proteins may be potential substrates of RNF114 with stabilization stemming from the nimbolide portion of XH2, as is likely the case with CDKN1A, CDKN1C, PEG10 and CTGF. The other targets may be downstream transcriptional effects stemming from JQ1-mediated BRD4 inhibition and degradation. Our results indicate that nimbolide reactivity with RNF114 can be exploited to recruit this E3 ligase to other protein substrates, such as BRD4, to ubiquitinate and selectively degrade them.

Covalent ligands against RNF114. With the insight gained that C8 of RNF114 has potential to be exploited for cancer therapy and targeted protein degradation applications, we searched for more synthetically tractable covalent ligands that similarly target RNF114. To achieve this goal, we screened a library of cysteine-reactive covalent ligands against RNF114 using a moderate-throughput gel-based ABPP approach, in which covalent ligands are competed against JNS27 labeling of RNF114, followed by appending a rhodamine-azide and analysis by SDS–PAGE and measuring in-gel fluorescence. Of the approximately 200 cysteine-reactive covalent ligands screened against RNF114, the acrylamide EN62 (11) emerged as a promising hit (Supplementary Fig. 5a,b, Supplementary Fig. 6a and Supplementary Dataset 4). EN62 inhibited RNF114 auto-ubiquitination activity in a C8-dependent manner (Supplementary Fig. 6b). While EN62 is an early hit compound that requires substantial improvements to cell permeability, potency and selectivity, this covalent ligand represents a starting point for more synthetically tractable covalent ligand scaffolds that target C8 of RNF114 for targeted protein degradation applications.

Discussion

Collectively, we show compelling evidence that nimbolide impairs breast cancer pathogenicity in part through targeting a substrate recognition domain at C8 in RNF114 to inhibit p21 ubiquitination and degradation, leading to its stabilization. We demonstrate that nimbolide targeting of C8 on RNF114 can be used to recruit RNF114 for targeted protein degradation applications and degradation of BRD4 with a nimbolide-JQ1 degrader XH2 is possible.

We report here that nimbolide disrupts RNF114 interactions with one of its endogenous substrate p21 and we also show that p21 levels are rapidly stabilized in breast cancer cells in a p53-independent manner. Several other E3 ligases have also been reported to degrade p21, including SCF^{SKP2}, $CRL4^{CDT2}$ and CHIP under varying conditions during cell cycle or exogenous stress[24–26]. Previous studies have shown that RNF114 expression is elevated at late G1 phase to regulate p21 and p57 levels and is crucial for G1-to-S phase transition[17]. Other RNF114 substrates that have been reported include TAB1 involved in maternal-to-zygotic transition and A20 involved in NF-κB activity and T cell activation[27,28]. In cancer contexts or other cell and tissue types, nimbolide may thus have additional activities through regulating the levels of other RNF114 protein substrates. We show CTGF and PEG10 may represent additional substrates of RNF114 as demonstrated by their nimbolide-induced stabilization in situ and poly-ubiquitination by RNF114 in vitro. Further studies are required to establish these additional proteins as direct and endogenous substrates of RNF114. Furthermore, while we show that RNF114 is one target of nimbolide that at least in part mediates its effects on proliferation and targeted protein degradation, we also show with the nimbolide-alkyne probe that nimbolide likely possesses many additional protein targets. These additional targets may include other covalent interactions with cysteines that are not labeled by the IA-alkyne cysteine-reactive probe in isoTOP-ABPP experiments, may represent covalent interactions with other amino acids, may represent reversible interactions with additional protein targets or may include proteins that are indirectly enriched from interactions with direct nimbolide-labeled proteins. Despite nimbolide possessing multiple potential targets, we demonstrate that RNF114 is an important and functional target of nimbolide in breast cancer cells that can be exploited for targeted protein degradation applications. We also convincingly show that the BRD4 degradation observed with the nimbolide-based degrader is driven through RNF114.

Our results also demonstrate that nimbolide functionally targets an intrinsically disordered region in RNF114. Solving the structure of RNF114 covalently modified with nimbolide has thus far proved to be challenging, but future studies investigating whether nimbolide induces order in the N terminus would provide insights into the ligandability of intrinsically disordered and undruggable protein targets and strategies for potentially targeting other E3 ligases.

Targeted protein degradation has emerged as a formidable and effective drug discovery model for targeting proteins for elimination through the proteasome[9,10]. One of the challenges, however, is that there are only a small number of E3 ligase recruiters that have been developed among the approximately 600 E3 ligases in the human genome[29]. These E3 ligase recruiters include the thalidomide-type immunomodulatory drugs that recruit cereblon, ligands that recruit VHL, nutlins that recruit MDM2 and ligands that recruit BIRC2 (cIAP)[9,10]. Here, we report that nimbolide can be used as a novel RNF114 recruiter for targeted protein degradation applications. It should be possible to optimize the performance of this degrader class through further linker modifications, an area of the molecule already determined to be important. It may also be possible to use more synthetically tractable covalent ligands capable of targeting C8 of RNF114, such as EN62, as RNF114 recruiters. Since nimbolide targets a substrate recognition domain in RNF114, it will also be of future interest to determine whether nimbolide may act as a molecular glue to recruit and degrade neo-substrates, as has been reported for the immunomodulatory drugs[30].

We did not observe degradation of BRD2 and BRD3 under conditions that led to significant reduction of BRD4 levels despite the high homology in their respective BET bromodomains. Various levels of selectivity in the BET family members and the structural basis thereof have been reported for JQ1-based degraders with Cereblon and VHL-recruiting modules[22,23,31,32]. While a more detailed investigation of the selectivity of XH2 and its structural basis is outside the scope of this study, it serves as another example of how availability of additional E3-moieties for a given substrate recognition modules can aid in tuning efficacy and selectivity of degraders targeting a given protein of interest.

Overall, our study further demonstrates the usefulness of ABPP-based chemoproteomic platforms in identifying unique druggable modalities exploited by natural products. We show that a natural product can functionally access an E3 ligase protein–protein interaction site for potential cancer therapy and targeted protein degradation applications and remarkably does so in an intrinsically disordered region of the protein. Our study also showcases how covalent ligand screening approaches can be used to identify more synthetically tractable small molecules that act similarly to more complex natural products and that covalent ligands may be able to access other E3 ligases to expand the scope of E3 ligase recruiters.

Online content

Any methods, additional references, Nature Research reporting summaries, source data, statements of code and data availability and associated accession codes are available at https://doi.org/10.1038/s41589-019-0304-8.

Received: 15 October 2018; Accepted: 8 May 2019;
Published online: 17 June 2019

References

1. Nomura, D. K. & Maimone, T. J. Target identification of bioactive covalently acting natural products. *Curr. Top. Microbiol. Immunol.* **420**, 351–374 (2018).
2. Drahl, C., Cravatt, B. F. & Sorensen, E. J. Protein-reactive natural products. *Angew. Chem. Int. Ed Engl.* **44**, 5788–5809 (2005).
3. Liu, J. et al. Calcineurin is a common target of cyclophilin-cyclosporin A and FKBP-FK506 complexes. *Cell* **66**, 807–815 (1991).
4. Cohen, E., Quistad, G. B. & Casida, J. E. Cytotoxicity of nimbolide, epoxyazadiradione and other limonoids from neem insecticide. *Life Sci.* **58**, 1075–1081 (1996).
5. Bodduluru, L. N., Kasala, E. R., Thota, N., Barua, C. C. & Sistla, R. Chemopreventive and therapeutic effects of nimbolide in cancer: the underlying mechanisms. *Toxicol. In Vitro* **28**, 1026–1035 (2014).
6. Subramani, R. et al. Nimbolide inhibits pancreatic cancer growth and metastasis through ROS-mediated apoptosis and inhibition of epithelial-to-mesenchymal transition. *Sci. Rep.* **6**, 19819 (2016).
7. Hao, F., Kumar, S., Yadav, N. & Chandra, D. Neem components as potential agents for cancer prevention and treatment. *Biochim. Biophys. Acta* **1846**, 247–257 (2014).
8. Gupta, S. C., Prasad, S., Tyagi, A. K., Kunnumakkara, A. B. & Aggarwal, B. B. Neem (Azadirachta indica): an Indian traditional panacea with modern molecular basis. *Phytomedicine* **34**, 14–20 (2017).
9. Burslem, G. M. & Crews, C. M. Small-molecule modulation of protein homeostasis. *Chem. Rev.* **117**, 11269–11301 (2017).
10. Lai, A. C. & Crews, C. M. Induced protein degradation: an emerging drug discovery paradigm. *Nat. Rev. Drug Discov.* **16**, 101–114 (2017).
11. Bianchini, G., Balko, J. M., Mayer, I. A., Sanders, M. E. & Gianni, L. Triple-negative breast cancer: challenges and opportunities of a heterogeneous disease. *Nat. Rev. Clin. Oncol.* **13**, 674–690 (2016).
12. Weerapana, E. et al. Quantitative reactivity profiling predicts functional cysteines in proteomes. *Nature* **468**, 790–795 (2010).
13. Roberts, A. M., Ward, C. C. & Nomura, D. K. Activity-based protein profiling for mapping and pharmacologically interrogating proteome-wide ligandable hotspots. *Curr. Opin. Biotechnol.* **43**, 25–33 (2017).
14. Grossman, E. A. et al. Covalent ligand discovery against druggable hotspots targeted by anti-cancer natural products. *Cell Chem. Biol.* **24**, 1368–1376.e4 (2017).
15. Backus, K. M. et al. Proteome-wide covalent ligand discovery in native biological systems. *Nature* **534**, 570–574 (2016).
16. Wang, C., Weerapana, E., Blewett, M. M. & Cravatt, B. F. A chemoproteomic platform to quantitatively map targets of lipid-derived electrophiles. *Nat. Methods* **11**, 79–85 (2014).
17. Han, J. et al. ZNF313 is a novel cell cycle activator with an E3 ligase activity inhibiting cellular senescence by destabilizingp21(WAF1.). *Cell Death Differ.* **20**, 1055–1067 (2013).
18. Lee, M.-G. et al. XAF1 directs apoptotic switch of p53 signaling through activation of HIPK2 and ZNF313. *Proc. Natl Acad. Sci. USA* **111**, 15532–15537 (2014).
19. Huang, S. et al. The UbL-UBA Ubiquilin4 protein functions as a tumor suppressor in gastric cancer by p53-dependent and p53-independent regulation of p21. *Cell Death Differ.* **26**, 516–530 (2019).
20. Abbas, T. & Dutta, A. p21 in cancer: intricate networks and multiple activities. *Nat. Rev. Cancer* **9**, 400–414 (2009).
21. Guo, H., Tian, T., Nan, K. & Wang, W. p57: a multifunctional protein in cancer (Review). *Int. J. Oncol.* **36**, 1321–1329 (2010).
22. Zengerle, M., Chan, K.-H. & Ciulli, A. Selective small molecule induced degradation of the BET bromodomain protein BRD4. *ACS Chem. Biol.* **10**, 1770–1777 (2015).
23. Winter, G. E. et al. Drug development. Phthalimide conjugation as a strategy for in vivo target protein degradation. *Science* **348**, 1376–1381 (2015).
24. Havens, C. G. & Walter, J. C. Mechanism of CRL4(Cdt2), a PCNA-dependent E3 ubiquitin ligase. *Genes Dev.* **25**, 1568–1582 (2011).
25. Kitagawa, K., Kotake, Y. & Kitagawa, M. Ubiquitin-mediated control of oncogene and tumor suppressor gene products. *Cancer Sci.* **100**, 1374–1381 (2009).
26. Biswas, K. et al. The E3 ligase CHIP mediates p21 degradation to maintain radioresistance. *Mol. Cancer Res.* **15**, 651–659 (2017).
27. Rodriguez, M. S. et al. The RING ubiquitin E3 RNF114 interacts with A20 and modulates NF-κB activity and T-cell activation. *Cell Death Dis.* **5**, e1399 (2014).
28. Yang, Y. et al. The E3 ubiquitin ligase RNF114 and TAB1 degradation are required for maternal-to-zygotic transition. *EMBO Rep.* **18**, 205–216 (2017).
29. Rape, M. Ubiquitylation at the crossroads of development and disease. *Nat. Rev. Mol. Cell Biol.* **19**, 59–70 (2018).
30. Hughes, S. J. & Ciulli, A. Molecular recognition of ternary complexes: a new dimension in the structure-guided design of chemical degraders. *Essays Biochem.* **61**, 505–516 (2017).
31. Gadd, M. S. et al. Structural basis of PROTAC cooperative recognition for selective protein degradation. *Nat. Chem. Biol.* **13**, 514–521 (2017).
32. Nowak, R. P. et al. Plasticity in binding confers selectivity in ligand-induced protein degradation. *Nat. Chem. Biol.* **14**, 706–714 (2018).

Acknowledgements

We thank the members of the Nomura Research Group, the Maimone laboratory and Novartis Institutes for BioMedical Research for critical reading of the manuscript. We acknowledge M. Moeller and A. Olding for assistance in nimbolide isolation studies. This work was supported by Novartis Institutes for BioMedical Research and the Novartis-Berkeley Center for Proteomics and Chemistry Technologies (NB-CPACT) for all listed authors. This work was also supported by grants from the National Institutes of Health (no. R01CA172667 for D.K.N., J.N.S., C.C.W. and L.O.; no. F31CA225173 for C.C.W.; no. F31CA239327 for J.N.S. and no. R01GM112948 for J.A.O.). This work was also supported by the Mark Foundation for Cancer Research ASPIRE award. J.A.O. is a Chan Zuckerberg Biohub investigator.

Author contributions

J.N.S., T.J.M. and D.K.N. conceived the project and wrote the paper. J.N.S., X.H., C.C.W., M.D.J., D.E.B., J.R.T., J.A.T., J.M.K., M.S., T.J.M. and D.K.N. provided intellectual contributions and insights into project direction. J.N.S., X.H., S.M.B., M.T., J.A.O., M.S., T.J.M. and D.K.N. designed the experiments and analyzed data. C.C.W. and M.D.J. developed bioinformatic methods and analyzed data for proteomics experiments. J.N.S., X.H., S.M.B., L.O., M.T., A.P., E.O., M.W. and D.K.N. performed experiments and analyzed data. A.P., E.O., M.W. and D.E.B. provided pure RNF114 protein. J.N.S., X.H. and T.J.M. designed and synthesized compounds. J.N.S., S.M.B., M.D.J., J.A.O., D.E.B., J.R.T., J.A.T., J.M.K., M.S., T.J.M. and D.K.N. edited the paper.

Competing interests

S.M.B., M.D.J., A.P., E.O., M.W., D.E.B., J.A.T., J.M.K. and M.S. are employees of Novartis Institutes for BioMedical Research. J.R.T. was an employee of Novartis Institutes for BioMedical Research when this study was submitted, but is now an employee of Vertex Pharmaceuticals. This study was funded by the Novartis Institutes for BioMedical Research and the Novartis-Berkeley Center for Proteomics and Chemistry Technologies. D.K.N. is a co-founder, share-holder and adviser for Artris Therapeutics and Frontier Medicines.

Additional information

Supplementary information is available for this paper at https://doi.org/10.1038/s41589-019-0304-8.

Reprints and permissions information is available at www.nature.com/reprints.

Correspondence and requests for materials should be addressed to T.J.M. or D.K.N.

Publisher's note: Springer Nature remains neutral with regard to jurisdictional claims in published maps and institutional affiliations.

Methods

Cell culture. The 231MFP cells were obtained from B. Cravatt and were generated from explanted tumor xenografts of MDA-MB-231 cells as previously described[33]. HCC38 and HEK293T cells were obtained from the American Type Culture Collection. HEK293T cells were cultured in DMEM containing 10% (v/v) fetal bovine serum (FBS) and maintained at 37 °C with 5% CO_2. The 231MFP cells were cultured in L15 medium containing 10% FBS and maintained at 37 °C with 0% CO_2. HCC38 cells were cultured in RPMI medium containing 10% FBS and maintained at 37 °C with 5% CO_2. HAP1 RNF114 wild-type and knockout cell lines were purchased from Horizon Discovery. The RNF114 knockout cell line was generated by CRISPR/Cas9 to contain a frameshift mutation in a coding exon of RNF114. HAP1 cells were grown in Iscove's Modified Dulbecco's Medium in the presence of 10% FBS and penicillin/streptomycin.

Survival and proliferation assays. Cell survival and proliferation assays were performed as previously described using Hoechst 33342 dye (Invitrogen) according to the manufacturer's protocol and as previously described[14]. The 231MFP cells were seeded into 96-well plates (40,000 for survival and 20,000 for proliferation) in a volume of 150 µl and allowed to adhere overnight. Cells were treated with an additional 50 µl of media containing 1:250 dilution of 1,000× compound stock in DMSO. After the appropriate incubation period, the media was removed from each well, and 100 µl of staining solution containing 10% formalin and Hoechst 33342 dye was added to each well and incubated for 15 min in the dark at room temperature. After incubation, staining solution was removed and wells were washed with PBS before imaging. Studies with HCC38 cells were also performed as above but were seeded with 20,000 cells for survival and 10,000 cells for proliferation.

Assessing apoptosis in breast cancer cells. Apoptotic cells were analyzed in cells treated with a DMSO vehicle or compound containing serum-free media for 24 or 48 h using flow cytometry. We measured the percentage of Annexin V-positive and propidium iodide-negative early apoptotic cells and Annexin V-positive and propidium iodide-positive late apoptotic cells as previously described[34]. We analyzed the data using FlowJo software.

IsoTOP-ABPP chemoproteomic studies. IsoTOP-ABPP studies were done as previously reported[12,14,15]. Cells were lysed by probe sonication in PBS and protein concentrations were measured by BCA assay[35]. For in situ experiments, cells were treated for 90 min with either DMSO vehicle or covalently acting small molecule (from 1,000× DMSO stock) before cell collection and lysis. Proteomes were subsequently labeled with IA-alkyne labeling (100 µM) for 1 h at room temperature. CuAAC was used by sequential addition of tris(2-carboxyethyl) phosphine (1 mM, Sigma), tris[(1-benzyl-1H-1,2,3-triazol-4-yl)methyl]amine (34 µM, Sigma), copper(II) sulfate (1 mM, Sigma) and biotin-linker-azide—the linker functionalized with a tobacco etch virus (TEV) protease recognition sequence as well as an isotopically light or heavy valine for treatment of control or treated proteome, respectively. After CuAAC, proteomes were precipitated by centrifugation at 6,500*g*, washed in ice-cold methanol, combined in a 1:1 control:treated ratio, washed again, then denatured and resolubilized by heating in 1.2% SDS–PBS to 80 °C for 5 min. Insoluble components were precipitated by centrifugation at 6,500*g* and soluble proteome was diluted in 5 ml 0.2% SDS–PBS. Labeled proteins were bound to avidin-agarose beads (170 µl resuspended beads per sample, Thermo Pierce) while rotating overnight at 4 °C. Bead-linked proteins were enriched by washing three times each in PBS and water, then resuspended in 6 M urea and PBS (Sigma), and reduced in TCEP (1 mM, Sigma), alkylated with iodoacetamide (18 mM, Sigma), before being washed and resuspended in 2 M urea and trypsinized overnight with 0.5 µg µl^{-1} sequencing grade trypsin (Promega). Tryptic peptides were eluted off. Beads were washed three times each in PBS and water, washed in TEV buffer solution (water, TEV buffer, 100 µM dithiothreitol) and resuspended in buffer with Ac-TEV protease and incubated overnight. Peptides were diluted in water and acidified with formic acid (1.2 M, Spectrum) and prepared for analysis.

Mass spectrometry analysis. Peptides from all chemoproteomic experiments were pressure-loaded onto a 250 µm inner diameter fused silica capillary tubing packed with 4 cm of Aqua C18 reverse-phase resin (Phenomenex no. 04A-4299), which was previously equilibrated on an Agilent 600 series high-performance liquid chromatograph using the gradient from 100% buffer A to 100% buffer B over 10 min, followed by a 5 min wash with 100% buffer B and a 5 min wash with 100% buffer A. The samples were then attached using a MicroTee PEEK 360 µm fitting (Thermo Fisher Scientific no. p-888) to a 13 cm laser pulled column packed with 10 cm Aqua C18 reverse-phase resin and 3 cm of strong-cation exchange resin for isoTOP-ABPP studies. Samples were analyzed using an Q Exactive Plus mass spectrometer (Thermo Fisher Scientific) using a five-step Multidimensional Protein Identification Technology (MudPIT) program, using 0, 25, 50, 80 and 100% salt bumps of 500 mM aqueous ammonium acetate and using a gradient of 5–55% buffer B in buffer A (buffer A: 95:5 water:acetonitrile, 0.1% formic acid; buffer B 80:20 acetonitrile:water, 0.1% formic acid). Data were collected in data-dependent acquisition mode with dynamic exclusion enabled (60 s). One full mass spectrometry (MS^1) scan (400–1,800 mass-to-charge ratio (m/z)) was followed by 15 MS^2 scans of the nth most abundant ions. Heated capillary temperature was set to 200 °C and the nanospray voltage was set to 2.75 kV.

Data were extracted in the form of 1 and MS^2 files using Raw Extractor v.1.9.9.2 (Scripps Research Institute) and searched against the Uniprot human database using ProLuCID search methodology in IP2 v.3 (Integrated Proteomics Applications, Inc.)[36]. Cysteine residues were searched with a static modification for carboxyaminomethylation (+57.02146) and up to two differential modifications for methionine oxidation and either the light or heavy TEV tags (+464.28596 or +470.29977, respectively). Peptides were required to be fully tryptic peptides and to contain the TEV modification. ProLUCID data were filtered through DTASelect to achieve a peptide false-positive rate below 5%. Only those probe-modified peptides that were evident across two out of three biological replicates were interpreted for their isotopic light to heavy ratios. For those probe-modified peptides that showed ratios greater than two, we only interpreted those targets that were present across all three biological replicates, were statistically significant and showed good quality MS^1 peak shapes across all biological replicates. Light versus heavy isotopic probe-modified peptide ratios are calculated by taking the mean of the ratios of each replicate paired light versus heavy precursor abundance for all peptide-spectral matches associated with a peptide. The paired abundances were also used to calculate a paired sample t-test P value in an effort to estimate constancy in paired abundances and significance in change between treatment and control. P values were corrected using the Benjamini–Hochberg method.

Knockdown of RNF114, CDKN1A (p21) and CDKN1C (p57) by RNA interference in 231MFP cells. RNA interference was performed by using siRNA purchased from Dharmacon specific to RNF114 or p21 and p57 for dual knockdown. In brief, 231MFP cells were seeded at a density of 5×10^4 cells per ml full media in a 96-well format. On day 0, 231MFP cells were transfected with corresponding siRNA versus non-targeting negative control (Dharmacon, ON-TARGETplus Non-targeting Pool D-001810-10-05) duplexes at 50 nM using Dharmafect 1 (Dharmacon) as a transfection reagent for 48 h. Thereafter (day 2), transfection media was supplemented with fresh DMSO or compound containing full L15 media and cultured for an additional 24–48 h before undergoing cell viability testing as described above. At the time of treatment (day 2), RNA was extracted for analysis by quantitative PCR with reverse transcription and lysates were obtained for western blotting confirmation of knockdown.

Targeting sequences:
siRNF114-1: GUGUGAAGGCCACCAUUAA (Dharmacon J-007024-08-0002)
siRNF114-2: GCUUAGAGGUGUACGAGAA (Dharmacon J-007024-05-0002)
siRNF114-3: GCACGGAUACCAAAUCUGU (Dharmacon J-007024-06-0002)
siCDKN1A: AGACCAGCAUGACAGAUUU (Dharmacon J-003471-12-0002)
siCDKN1C: CUGAGAAGUCGUCGGGCGA (Dharmacon J-003244-13-0002)

Gene expression by quantitative PCR. Total RNA was extracted from cells using Trizol (Thermo Fisher Scientific). Complementary DNA was synthesized using MaximaRT (Thermo Fisher Scientific) and gene expression was confirmed by quantitative PCR (qPCR) using the manufacturer's protocol for Fisher Maxima SYBR Green (Thermo Fisher Scientific) on the CFX Connect Real-Time PCR Detection System (Bio-Rad). Primer sequences for Fisher Maxima SYBR Green were derived from Primer Bank. Sequences of primers are as follows:

RNF114 Forward: AAT GTT CCA AAC CG
RNF114 Reverse: TTG CAG TGT TCC AC
CDKN1A Forward: TGT CCG TCA GAA CCC ATG C
CDKN1A Reverse: AAA GTC GAA GTT CCA TCG CTC
PPIA (Cyclophilin) Forward: CCC ACC GTG TTC TTC GAC ATT
PPIA (Cyclophilin) Reverse: GGA CCC GTA TGC TTT AGG ATG A

Gel-based ABPP. Gel-based ABPP methods were performed as previously described[14]. Recombinant pure human proteins were purchased from Origene. Pure proteins (0.1 µg) were pre-treated with DMSO vehicle or covalently acting small molecules for 30 min at room temperature in an incubation volume of 50 µl PBS, and were subsequently treated with JNS-1-27 (50 µM final concentration) for 1 h at room temperature. CuAAC was performed to append rhodamine-azide (1 µM final concentration) onto alkyne probe-labeled proteins. Samples were then diluted with 20 µl of 4× reducing Laemmli SDS sample loading buffer (Alfa Aesar) and heated at 90 °C for 5 min. The samples were separated on precast 4–20% TGX gels (Bio-Rad Laboratories, Inc.). Before scanning by ChemiDoc MP (Bio-Rad Laboratories, Inc.), gels were fixed in a solution of 10% acetic acid, 30% ethanol for 2 h. Inhibition of target labeling was assessed by densitometry using ImageJ.

Synthesis and characterization of the nimbolide-alkyne probe and degraders XH1 and XH2. See Supplementary Information for experimental details.

Synthesis and characterization of JNS27. See Supplementary Information for experimental details.

Covalent ligand library. The synthesis and characterization of most of the covalent ligands screened against RNF114 have been previously reported[14,37–39].

Syntheses of TRH 1-156, TRH 1-160, TRH 1-167, YP 1-16, YP 1-22, YP 1-26, YP 1-31 and YP 1-44 have been previously reported[40–47]. Compounds starting with 'EN' were purchased from Enamine LLC. The synthesis and characterization of other covalent ligands not previously reported are described in Supplementary Information.

Western blotting. Antibodies to RNF114 (Millipore Sigma, HPA021184), p21 (Cell Signaling Technology, 12D1), GAPDH (Proteintech Group Inc., 60004-1-Ig), BRD4 (Abcam plc, Ab128874), DYKDDDDK Tag (Cell Signaling Technology, D6W5B) and beta-actin (Proteintech Group Inc., 6609-1-Ig) were obtained from various commercial sources and dilutions were prepared per the recommended manufacturers' procedures. Proteins were resolved by SDS–PAGE and transferred to nitrocellulose membranes using the iBlot system (Invitrogen). Blots were blocked with 5% BSA in Tris-buffered saline containing Tween 20 (TBST) solution for 1 h at room temperature, washed in TBST and probed with primary antibody diluted in diluent, as recommended by the manufacturer, overnight at 4 °C. Following washes with TBST, the blots were incubated in the dark with secondary antibodies purchased from Ly-Cor and used at 1:10,000 dilution in 5% BSA in TBST at room temperature. Blots were visualized using an Odyssey Li-Cor scanner after additional washes. If additional primary antibody incubations were required, the membrane was stripped using ReBlot Plus Strong Antibody Stripping Solution (EMD Millipore, 2504), washed and blocked again before being reincubated with primary antibody.

Expression and purification of wild-type and C8A mutant RNF114 protein. RNF114 was expressed and purified using several methods. In each case, RNF114 activity and sensitivity to nimbolide was confirmed. For the first method, we purchased wild-type mammalian expression plasmids with a C-terminal FLAG tag were purchased from Origene (Origene Technologies Inc., RC209752). The RNF114 C8A mutant was generated with Q5 site-directed mutagenesis kit according to the manufacturer's instructions (New England Biolabs, E0554S). Expression and purification conditions were optimized as reported previously[48]. HEK293T cells were grown to 60% confluency in DMEM (Corning) supplemented with 10% FBS (Corning) and 2 mM L-glutamine (Life Technologies) and maintained at 37 °C with 5% CO_2. Immediately before transfection, media was replaced with DMEM containing 5% FBS. Each plate was transfected with 20 µg of overexpression plasmid with 100 µg poly(ethyleneimine)(Sigma). After 48 h cells were collected in TBS, lysed by sonication and batch bound with anti-DYKDDDDK resin (GenScript, L00432) for 90 min. Lysate and resin was loaded onto a gravity flow column and washed, followed by elution with 250 ng µl^{-1} 3XFLAG peptide (ApexBio, A6001). Purity and concentration were verified by PAGE, ultraviolet spectroscopy and BCA assay.

For the second method, DNA encoding the complete human isoform of RNF114 (Uniprot ID Q9Y508) was codon optimized for expression in *Escherichia coli* and synthesized by Integrated DNA Technologies. Constructs containing the complete RNF114 sequence were amplified using primers containing 20 base pair homology to a pET24a plasmid (Novagen) that also contained a His_8-MBP-TEV sequence between Nde1 and BamH1 restriction sites. Products for PCR were assessed using 1% agarose gels (Invitrogen), and a QIAquick Gel Extraction kit (Qiagen) was used to purify PCR products of the correct length. Gibson Assembly (NEB Gibson Assembly 2× Master Mix) was used to assemble the purified PCR product into the linearized vector. This vector was then transformed into chemically competent *E. coli* 10G cells (Lucigen). Kanamycin (Kan)-resistant colonies were grown in LB media and a Miniprep (Qiagen) kit was used to isolate the plasmid before sequence verification with appropriate primers.

pET24a His_8–MBP plasmid (100 ng) containing the desired RNF114 construct was transformed into chemically competent *E. coli* BL21(DE3) cells (NEB product no. C2530H). The following day, a single transformed colony was used to inoculate 50 ml of nutrient rich LB medium containing kanamycin (50 µg ml^{-1}) and was incubated at 37 °C overnight, with agitation (250 r.p.m.). The following morning, an overnight starter culture was inoculated to a starting optical density at 500 nM (OD_{600}) of 0.1 in Terrific Broth (TB) (1 l) containing 50 mM 3-(*N*-morpholino)propanesulfonic acid pH 7.5, 1 mM zinc chloride and Kan (50 µg ml^{-1}). Cells were grown until achieving an OD_{600} of 0.8 at 37 °C with agitation at 250 r.p.m. At this stage, expression of the RNF114 fusion protein was induced with 1 mM isopropyl β-D-1-thiogalactopyranoside and the temperature of the incubator was reduced to 18 °C. Cells were collected by centrifugation after growth for 18 h at 18 °C. Cells were subsequently washed with 1× PBS buffer and stored at −20 °C.

E. coli cells (10 g) containing the overexpressed RNF114 fusion protein were resuspended in 80 ml of lysis buffer (50 mM Tris, pH 7.5, 150 mM NaCl, two Roche protease inhibitor tablets (without EDTA), 200 mM $ZnCl_2$, 1 mM DTT) and sonicated on ice, with a cycling time of 60 s on, 60 s off, over a total sonication time of 3 min. The cell lysate was centrifuged at 18,000 r.p.m. for 20 min and the soluble protein was incubated with agitation for 4 h at 4 °C with 2 ml of Ni-NTA resin, which had been pre-equilibrated with wash buffer (50 mM Tris, pH 7.5, 150 mM NaCl, 200 mM $ZnCl_2$, 1 mM DTT, 25 mM imidazole). The cell lysate/Ni-NTA resin mixture was placed into a disposable column and all non-tagged soluble protein, which do not bind to the resin, was collected for a second round of purification. The resin was washed with 25 ml of wash buffer before the His-MBP-RNF114 protein was eluted from the Ni-NTA resin with 25 ml of elution buffer (50 mM tris, pH 7.5, 500 mM imidazole, 200 mM $ZnCl_2$, 150 mM NaCl, 1 mM DTT). This process was repeated incubating the collected flow thorough with an additional 2 ml of pre-equilibrated Ni-NTA resin.

His-MBP-RNF114 protein was simultaneously digested at 4 °C with TEV protease (100 units per mg MBP-RNF114) and dialyzed overnight against dialysis buffer (50 mM tris, pH 7.5, 150 mM NaCl, 200 mM $ZnCl_2$, 1 mM DTT). The following morning two 5 ml His Trap Excel columns assembled in tandem were placed on an Äkta Avant and equilibrated with five column volumes of wash buffer. The TEV cleaved sample was loaded onto the column at a rate of 2 ml min^{-1} and the resin was washed with an additional five column volumes of wash buffer. All fractions containing cleaved RNF114 were concentrated to a 5 ml volume. Samples were then loaded onto a pre-equilibrated HiLoad 16/60 Superdex 75 gel filtration column (GE Healthcare). Columns were pre-equilibrated with either 25 mM Tris, pH 7.5, 137 mM NaCl, or 20 mM sodium phosphate pH 6.8, 150 mM NaCl. The gel filtration column was run using a flow rate of 0.25 ml min^{-1} and 2 ml fractions were collected. Fractions corresponding to peaks eluting from the gel filtration column were analyzed using SDS–PAGE and all fractions containing RNF114 were concentrated to a final concentration of 10 mg ml^{-1}, flash frozen in liquid nitrogen and stored at −80 °C until needed.

Generation of stably expressing FLAG-RNF114 231MFP cell lines by lentiviral transduction. Human RNF114 with C-terminal FLAG tag was inserted into pLenti vector by FastCloning[49]. FLAG-RNF114 lentivirus was generated by co-transfection of FLAG-RNF114, VSV.G and psPAX2 into HEK 293T cells using Lipfectamine 2000 transfection reagent (Thermo Fisher). Then, 24 h after transfection, the media was exchanged for DMEM with 10% heat-inactivated serum (HIS), and after an additional 24 h virus-containing media was collected and filtered with 0.45 µM filter onto 231MFP cells with equal volume HIS L15 media in the presence of 10 µg ml^{-1} polybrene (Santa Cruz). Twenty-four hours after transduction, puromycin (2 µg ml^{-1}) was added to cells and stably expressing FLAG-RNF114 cells were obtained after puromycin selection for 72 h. The 231MFP cells stably expressing FLAG-eGFP were generated in parallel as a control.

In situ nimbolide-alkyne probe labeling and FLAG-RNF114 pulldown. The 231MFP cells stably expressing FLAG-RNF114 were treated with either DMSO vehicle or 100 nM to 10 µM nimbolide-alkyne probe for 2–4 h. Cells were collected in PBS and lysed by sonication. Total protein concentration of lysates was normalized by BCA assay and normalized lysates were incubated 1.5 h at 4 °C with 50 µl or FLAG agarose slurry. After incubation, samples were transferred to spin columns and washed three times with 500 µl PBS. Proteins were eluted using two 50 µl washes of PBS supplemented with 250 ng µl^{-1} 3XFLAG peptide (ApexBio A6001). CuAAC was performed to append rhodamine-azide onto alkyne probe-labeled proteins and after addition of loading buffer samples were separated on precast 4–20% TGX gels (Bio-Rad Laboratories, Inc.) and imaged on ChemiDoc MP (Bio-Rad Laboratories, Inc.).

LC–MS/MS analysis of RNF114. Purified RNF114 (10 µg) in 50 µl PBS were incubated 30 min at room temperature either with DMSO vehicle or covalently acting compound (100 µM). The DMSO control was then treated with light iodoacetamide while the compound treated sample was incubated with heavy iodoacetamide for 1 h each at room temperature (200 µM final concentration, Sigma-Aldrich, 721328). The samples were precipitated by additional of 12.5 µl of 100% (w/v) trichloroacetic acid and the treated and control groups were combined pairwise, before cooling to −80 °C for 1 h. The combined sample was then spun for at max speed for 10 min at 4 °C, supernatant was carefully removed and the sample was washed with ice-cold 0.01 M HCl/90% acetone solution. The pellet was resuspended in 4 M urea containing 0.1% Protease Max (Promega Corp. V2071) and diluted in 40 mM ammonium bicarbonate buffer. The samples were reduced with 10 mM TCEP at 60 °C for 30 min. The sample was then diluted 50% with PBS before sequencing grade trypsin (1 µg per sample, Promega Corp, V5111) was added for an overnight incubation at 37 °C. The next day, the sample was centrifuged at 13,200 r.p.m. for 30 min. The supernatant was transferred to a new tube and acidified to a final concentration of 5% formic acid and stored at −80 °C until mass spectrometry analysis.

RNF114 ubiquitination assay. Recombinant Myc-Flag-RNF114 proteins were either purified from HEK292T cells as described above or purchased from Origene (Origene Technologies Inc., TP309752). For in vitro auto-ubiquitination assay, 0.2 µg of RNF114 in 25 µl of TBS was pre-incubated with DMSO vehicle or the covalently acting compound for 30 min at room temperature. Subsequently, 0.1 µg of UBE1 (Boston Biochem. Inc., E-305), 0.1 µg UBE2D1 (Boston Bichem. Inc., e2-615), 5 µg of Flag-ubiquitin (Boston Bichem. Inc., u-120) in a total volume of 25 µl Tris buffer containing 2 mM ATP, 10 mM DTT and 10 mM $MgCl_2$ were added to achieve a final volume of 50 µl. For substrate-protein ubiquitination assays, 0.1 µg of the appropriate substrate protein, purchased from commercial sources, was

added at this stage (p21 and PEG10: Origene, CTGF: R&D Systems). The mixture was incubated at 37 °C with agitation for 1.5 h. Then, 20 µl of Laemmli's buffer was added to quench the reaction and proteins were analyzed by western blot assay.

RNF114/p21 co-immunoprecipitation. Recombinant Flag-tagged RNF114 was used as bait to precipitate pure recombinant p21 (Origene Technologies Inc., TP309752 and TP720567) using Anti-Flag agarose beads (GenScript Biotech Corp., L00432). One microgram of Flag-RNF114 was added to 50 µl of TBS, followed by the addition of nimbolide (100 µM final concentration, Cayman Chemical Co., 19230) or equivalent volume of DMSO. Samples were incubated at room temperature for 30 min. One microgram of pure p21 was added to each sample and samples were incubated at room temperature 30 min with agitation. Ten microliters of Flag agarose beads were added to each sample and samples were agitated at room temperature for 30 min. Washes (three times, 1 ml TBS) were performed before proteins were eluted using 50 µl of TBS supplemented with 250 ng µl^{-1} 3XFLAG peptide (ApexBio A6001). Supernatant (30 µl) were collected and after the addition of Laemmli's reducing agent (10 µl), samples were boiled at 95 °C for 5 min and allowed to cool. Samples were analyzed by western blotting as described above.

In situ nimbolide-alkyne probe labeling and biotin-azide pulldown. Experiments were performed following an adaption of a previously described protocol[50]. The 231MFP cells were treated with either DMSO vehicle or 50 µM nimbolide-alkyne probe for 90 min. Cells were collected in PBS and lysed by sonication. For preparation of western blotting sample, 195 µl of lysate was aliquoted per sample to which 25 µl of 10% SDS, 5 µl of 5 mM biotin picolylazide (900912 Sigma-Aldrich) and 25 µl of click reaction mix (three parts TBTA 5 mM TBTA in butanol:DMSO (4:1, v/v), one part 50 mM Cu(II)SO_4 solution and one part 50 mM TCEP). Samples were incubated for 2 h at 37 °C with gentle agitation after which 1.2 ml ice-cold acetone were added. After overnight precipitation at −20 °C, samples were spun in a prechilled centrifuge at 1,250*g* for 10 min allowing for aspiration of excess acetone and subsequent reconstitution of protein pellet in 200 µl PBS containing 1% SDS by probe sonication. At this stage, total protein concentration was determined by BCA assay and samples were normalized to a total volume of 230 µl, with 30 µl reserved as input. Then 20 µl of prewashed 50% streptavidin agarose bead slurry was added to each sample and samples were incubated overnight at room temperature with gentle agitation. Supernatant was aspirated from each sample after spinning at 90*g* for 2 min at room temperature. Beads were transferred to spin columns and washed three times with PBS. To elute, beads were boiled 5 min in 50 µl LDS sample buffer. Eluents were collected by centrifugation and analyzed by immunoblotting.

The resulting samples were analyzed as described below in the TMT-based quantitative proteomic profiling section.

TMT-based quantitative proteomic profiling. *Cell lysis, proteolysis and Isobaric labeling.* Treated cell-pellets were lysed and digested using the commercially available Pierce Mass Spec Sample Prep Kit for Cultured Cells (Thermo Fisher Scientific, P/N 84840) following the manufacturer's instructions. Briefly, 100 µg protein from each sample was reduced, alkylated and digested overnight using a combination of Endoproteinase Lys-C and trypsin proteases. Individual samples were then labeled with isobaric tags using commercially available TMTsixplex (Thermo Fisher Scientific, P/N 90061) or TMT11plex (TMT11plex) isobaric labeling reagent (Thermo Fisher Scientific, P/N 23275) kits, in accordance with the manufacturer's protocols.

High-pH reversed phase separation. TMT-labeled samples were then consolidated and separated using high-pH reversed phase chromatography (RP-10) with fraction collection as previously described[50]. Fractions were speed-vacuum dried, then reconstituted to produce 24 fractions for subsequent online nanoLC–MS/MS analysis.

Protein identification and quantitation by nanoLC–MS/MS. Reconstituted RP-10 fractions were analyzed on a Thermo Orbitrap Fusion Lumos Mass Spectrometer (Xcalibur 4.1, Tune Application v.3.0.2041) coupled to an EasyLC 1200 high-performance liquid chromatography system (Thermo Fisher Scientific). The EasyLC 1200 was equipped with a 20 µl loop, set-up for 96-well plates. A Kasil-fritted trapping column (75 µm ID) packed with ReproSil-Pur 120 C18-AQ, 5 µm material (15 mm bed length) was used together with a 160 mm length, 75 µm inner diameter spraying capillary pulled to a tip diameter of approximately 8–10 µm using a P-2000 capillary puller (Sutter Instruments). The 160 mm separation column was packed with ReproSil-Pur 120 C18-AQ, 3 µm material (Dr. Maisch). Mobile phase consisted of A, 0.1% formic acid/2% acetonitrile (v/v), and mobile phase B, 0.1% formic acid/98% acetonitrile (v/v). Samples (18 µl) were injected on to trapping column using mobile phase A at a flow rate of 2.5 µl min. Peptides were then eluted using an 80 min gradient (2% mobile phase B for 5 min, 2–40% B from 5–65 min, followed by 70% B from 65 to 70 min, then returning to 2% B from 70–80 min) at a flow rate of 300 nl min^{-1} on the capillary separation column with direct spraying into the mass spectrometer. Data were acquired on Orbitrap Fusion Lumos Mass Spectrometer in data-dependent mode using synchronous precursor scanning MS^3 mode (SPS–MS3), with MS^2 triggered for the 12 most intense precursor ions inside a *m/z* range of 300–1,500 found in the full mass spectrometry survey scan event. Mass spectrometry scans were acquired at 60,000 mass resolution (*R*) at *m/z* 400, using a target value of 4×10^5 ions and a maximum fill time of 50 ms. MS^2 scans were acquired as CID ion trap rapid type scans using a target value of 1×10^4 ions, maximum fill time of 50 ms and an isolation window of 2 Da. Data-dependent MS^3 spectra were acquired as Orbitrap (scans, using Top 10 MS^2 daughter selection, automatic gain control target of 5×10^4 ions, with scan range of *m/z* 100–500. The MS^3 maximum injection time was 86 ms, with higher-energy collision dissociation energy set to 65%. MS^3 mass resolution (*R*) was set to 15,000 at *m/z* 400 for TMT6plex experiments and 50,000 at *m/z* 400 for TMT11plex experiments. Dynamic exclusion was set to exclude selected precursors for 60 s with a repeat count of one. Nanospray voltage was set to 2.2 kV, with heated capillary temperature set to 300 °C and an S-lens radio frequency (RF) level equal to 30%. No sheath or auxiliary gas flow was applied.

Data processing and analysis. Acquired mass spectrometry data were processed using Proteome Discoverer v.2.2.0.388 software (Thermo Fisher) using the Mascot v.2.5.1 search engine (Matrix Science) together with Percolator validation node for peptide-spectral match filtering[51]. Data were searched against Uniprot protein database (canonical human and mouse sequences, EBI) supplemented with sequences of common contaminants. Peptide search tolerances were set to 10 ppm for precursors and 0.8 Da for fragments. Trypsin cleavage specificity (cleavage at lysine (K), arginine (R) except if followed by P) allowed for up to two missed cleavages. Carbamidomethylation of cysteine was set as a fixed modification, methionine oxidation and TMT-modification of N termini and lysine residues were set as variable modifications. Data validation of peptide and protein identifications was done at the level of the complete dataset consisting of combined Mascot search results for all individual samples per experiment via the Percolator validation node in Proteome Discoverer. Reporter ion ratio calculations were performed using summed abundances with most confident centroid selected from 20 ppm window. Only peptide-to-spectrum matches that are unique assignments to a given identified protein inside the total dataset are considered for protein quantitation. High-confidence protein identifications were reported using a Percolator estimated <1% false discovery rate cut-off. Differential abundance significance was estimated using a background-based analysis of variance with Benjamini–Hochberg correction to determine adjusted *P* values.

Reporting Summary. Further information on research design is available in the Nature Research Reporting Summary linked to this article.

Data availability

The datasets generated during and/or analyzed during the current study are available from the corresponding author on reasonable request.

References

33. Jessani, N. et al. Carcinoma and stromal enzyme activity profiles associated with breast tumor growth in vivo. *Proc. Natl Acad. Sci. USA* **101**, 13756–13761 (2004).
34. Anderson, K. E., To, M., Olzmann, J. A. & Nomura, D. K. Chemoproteomics-enabled covalent ligand screening reveals a thioredoxin-caspase 3 interaction disruptor that impairs breast cancer pathogenicity. *ACS Chem. Biol.* **12**, 2522–2528 (2017).
35. Smith, P. K. et al. Measurement of protein using bicinchoninic acid. *Anal. Biochem.* **150**, 76–85 (1985).
36. Xu, T. et al. ProLuCID: an improved SEQUEST-like algorithm with enhanced sensitivity and specificity. *J. Proteomics* **129**, 16–24 (2015).
37. Bateman, L. A. et al. Chemoproteomics-enabled covalent ligand screen reveals a cysteine hotspot in reticulon 4 that impairs ER morphology and cancer pathogenicity. *Chem. Commun. (Camb.)* **53**, 7234–7237 (2017).
38. Counihan, J. L.., Wiggenhorn, A. L.., Anderson, K. E.. & Nomura, D. K.. Chemoproteomics-enabled covalent ligand screening reveals ALDH3A1 as a lung cancer therapy target. *ACS Chem. Biol.* **13**, 1970–1977 (2018).
39. Roberts, A. M. et al. Chemoproteomic screening of covalent ligands reveals UBA5 As a novel pancreatic cancer target. *ACS Chem. Biol.* **12**, 899–904 (2017).
40. Kokosza, K., Balzarini, J. & Piotrowska, D. G. Novel 5-arylcarbamoyl-2-methylisoxazolidin-3-yl-3-phosphonates as nucleotide analogues. *Nucleosides Nucleotides Nucleic Acids* **33**, 552–582 (2014).
41. Talaty, E. R., Young, S. M., Dain, R. P. & Stipdonk, M. J. V. A study of fragmentation of protonated amides of some acylated amino acids by tandem mass spectrometry: observation of an unusual nitrilium ion. *Rapid Commun. Mass Spectrom.* **25**, 1119–1129 (2011).

42. Timokhin, V. I., Gastaldi, S., Bertrand, M. P. & Chatgilialoglu, C. Rate constants for the β-elimination of tosyl radical from a variety of substituted carbon-centered radicals. *J. Org. Chem.* **68**, 3532–3537 (2003).
43. Cee, V. J. et al. Systematic study of the glutathione (GSH) reactivity of *N*-arylacrylamides: 1. Effects of aryl substitution. *J. Med. Chem.* **58**, 9171–9178 (2015).
44. Le Sann, C., Huddleston, J. & Mann, J. Synthesis and preliminary evaluation of novel analogues of quindolines as potential stabilisers of telomeric G-quadruplex DNA. *Tetrahedron* **63**, 12903–12911 (2007).
45. Ikoma, M., Oikawa, M. & Sasaki, M. Synthesis and domino metathesis of functionalized 7-oxanorbornene analogs toward *cis*-fused heterocycles. *Tetrahedron* **64**, 2740–2749 (2008).
46. Cho, S.-D. et al. A one-pot synthesis of pyrido[2,3-b][1,4]oxazin-2-ones. *J. Org. Chem.* **68**, 7918–7920 (2003).
47. Magolan, J., Carson, C. A. & Kerr, M. A. Total synthesis of (±)-mersicarpine. *Org. Lett.* **10**, 1437–1440 (2008).
48. Longo, P. A., Kavran, J. M., Kim, M.-S. & Leahy, D. J. Transient mammalian cell transfection with polyethylenimine (PEI). *Methods Enzymol* **529**, 227–240 (2013).
49. Li, C. et al. FastCloning: a highly simplified, purification-free, sequence- and ligation-independent PCR cloning method. *BMC Biotechnol.* **11**, 92 (2011).
50. Thomas, J. R. et al. A photoaffinity labeling-based chemoproteomics strategy for unbiased target deconvolution of small molecule drug candidates. *Methods Mol. Biol.* **1647**, 1–18 (2017).
51. Käll, L., Canterbury, J. D., Weston, J., Noble, W. S. & MacCoss, M. J. Semi-supervised learning for peptide identification from shotgun proteomics datasets. *Nat. Methods* **4**, 923–925 (2007).

nature research

Corresponding author(s): Daniel Nomura and Thomas Maimone

Last updated by author(s): Apr 20, 2019

Reporting Summary

Nature Research wishes to improve the reproducibility of the work that we publish. This form provides structure for consistency and transparency in reporting. For further information on Nature Research policies, see Authors & Referees and the Editorial Policy Checklist.

Statistics

For all statistical analyses, confirm that the following items are present in the figure legend, table legend, main text, or Methods section.

n/a	Confirmed	
☐	☒	The exact sample size (*n*) for each experimental group/condition, given as a discrete number and unit of measurement
☐	☒	A statement on whether measurements were taken from distinct samples or whether the same sample was measured repeatedly
☐	☒	The statistical test(s) used AND whether they are one- or two-sided *Only common tests should be described solely by name; describe more complex techniques in the Methods section.*
☒	☐	A description of all covariates tested
☐	☒	A description of any assumptions or corrections, such as tests of normality and adjustment for multiple comparisons
☐	☒	A full description of the statistical parameters including central tendency (e.g. means) or other basic estimates (e.g. regression coefficient) AND variation (e.g. standard deviation) or associated estimates of uncertainty (e.g. confidence intervals)
☐	☒	For null hypothesis testing, the test statistic (e.g. *F*, *t*, *r*) with confidence intervals, effect sizes, degrees of freedom and *P* value noted *Give P values as exact values whenever suitable.*
☒	☐	For Bayesian analysis, information on the choice of priors and Markov chain Monte Carlo settings
☒	☐	For hierarchical and complex designs, identification of the appropriate level for tests and full reporting of outcomes
☒	☐	Estimates of effect sizes (e.g. Cohen's *d*, Pearson's *r*), indicating how they were calculated

Our web collection on statistics for biologists contains articles on many of the points above.

Software and code

Policy information about availability of computer code

Data collection	IP2-Integrated Proteomics Pipeline version 5.0.1 was used to analyze chemoproteomics data; Proteome Discoverer v.2.2.0.388 was used for other proteomics data
Data analysis	IP2-Integrated Proteomics Pipeline version 5.0.1 was used to analyze chemoproteomics data; Proteome Discoverer v.2.2.0.388 was used for other proteomics data

For manuscripts utilizing custom algorithms or software that are central to the research but not yet described in published literature, software must be made available to editors/reviewers. We strongly encourage code deposition in a community repository (e.g. GitHub). See the Nature Research guidelines for submitting code & software for further information.

Data

Policy information about availability of data

All manuscripts must include a data availability statement. This statement should provide the following information, where applicable:

- Accession codes, unique identifiers, or web links for publicly available datasets
- A list of figures that have associated raw data
- A description of any restrictions on data availability

We have provided Supplementary Datasets 1-3 for our complete proteomic data, in which UniProt IDs are provided for the proteins detected in the experiments.

Field-specific reporting

Please select the one below that is the best fit for your research. If you are not sure, read the appropriate sections before making your selection.

☒ Life sciences ☐ Behavioural & social sciences ☐ Ecological, evolutionary & environmental sciences

For a reference copy of the document with all sections, see nature.com/documents/nr-reporting-summary-flat.pdf

Life sciences study design

All studies must disclose on these points even when the disclosure is negative.

Sample size	No statistical analysis was performed to determine sample sizes. The sample sizes in the study were chosen based on prior knowledge on the intrinsic variability of the experiments performed.
Data exclusions	No data were excluded.
Replication	All the experiments were performed at least twice and the trends were reproducible between experiments. The covalent ligand screen was done with an n=1, but the apparent hits were reproduced in a second experiment and the lead compound dose-response was repeated with an n=3
Randomization	The cells used in the study were not randomized as this was not practical for experimental design.
Blinding	Investigators were not blinded to the study. Experimental data are precise measurements of protein levels and are not subjective measurements.

Reporting for specific materials, systems and methods

We require information from authors about some types of materials, experimental systems and methods used in many studies. Here, indicate whether each material, system or method listed is relevant to your study. If you are not sure if a list item applies to your research, read the appropriate section before selecting a response.

Materials & experimental systems

n/a	Involved in the study
☐	☒ Antibodies
☐	☒ Eukaryotic cell lines
☒	☐ Palaeontology
☒	☐ Animals and other organisms
☒	☐ Human research participants
☒	☐ Clinical data

Methods

n/a	Involved in the study
☒	☐ ChIP-seq
☐	☒ Flow cytometry
☒	☐ MRI-based neuroimaging

Antibodies

Antibodies used	RNF114 (Millipore Sigma, HPA021184), p21 (Cell Signaling Technology, 12D1), GAPDH (Proteintech Group Inc., 60004-1-Ig), BRD4 (Abcam plc, Ab128874), DYKDDDDK Tag (Cell Signaling Technology, D6W5B) and beta-actin (Proteintech Group Inc., 6609-1-Ig)
Validation	Antibodies validated by manufacturer

Eukaryotic cell lines

Policy information about cell lines

Cell line source(s)	231MFP cells were derived as described in PNAS 101, 13756-13761, HCC38 and HEK293T cells were purchased from ATCC, HAP1 cells were purchased from Horizon Discovery
Authentication	231MFP cells were derived as described in PNAS 101, 13756-13761, Other lines have been validated by ATCC and Horizon Discovery
Mycoplasma contamination	Mycoplasma contamination All the cell line used were tested and found to be negative for mycoplasma contamination
Commonly misidentified lines (See ICLAC register)	No commonly misidentified lines were used.

Flow Cytometry

Plots

Confirm that:

☒ The axis labels state the marker and fluorochrome used (e.g. CD4-FITC).

☒ The axis scales are clearly visible. Include numbers along axes only for bottom left plot of group (a 'group' is an analysis of identical markers).

☒ All plots are contour plots with outliers or pseudocolor plots.

☒ A numerical value for number of cells or percentage (with statistics) is provided.

Methodology

Sample preparation	Apoptotic cells were analyzed in cells treated with DMSO vehicle or compound containing serum-free media for 24 or 48 h using flow cytometry. We measured the percentage of Annexin V-positive and propidium iodide-negative early apoptotic cells and Annexin V-positive and propidium iodide-positive late apoptotic cells as previously described in ACS Chem Biol 12, 2522-2528
Instrument	BD LSRFortessa
Software	Data analysis was performed using FlowJo software.
Cell population abundance	10,000 single cells were analyzed and positive / negative staining visualized in 2-dimensional pseudocolor plots.
Gating strategy	Single cells were manually gated based on the FSC/SSC, and boundaries for positive and negative staining cell populations defined using untreated control cells. An example of the gating strategy used is shown in Fig SXX. The boundaries for positive and negative staining are shown in each figure (Fig. 1C, Fig. S1B)

☒ Tick this box to confirm that a figure exemplifying the gating strategy is provided in the Supplementary Information.